

# Warm Inflation in Hybrid Model



By

Waqar Ahmad

(Registration No: 00000365272)

Department of Physics

School of Natural Sciences

National University of Sciences and Technology (NUST)

Islamabad, Pakistan

(2024)

# Warm Inflation in Hybrid Model



By

Waqar Ahmad

(Registration No: 00000365272)

A thesis submitted to the National University of Sciences and Technology, Islamabad,

in partial fulfillment of the requirements for the degree of

Master of Science in

Physics

Supervisor: Dr. Saadi Ishaq

School of Natural Sciences


National University of Sciences and Technology (NUST)

Islamabad, Pakistan

(2024)

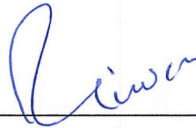
## THESIS ACCEPTANCE CERTIFICATE

Certified that final copy of MS thesis written by Waqar Ahmad (Registration No. 00000365272), of School of Natural Sciences has been vetted by undersigned, found complete in all respects as per NUST statutes/regulations, is free of plagiarism, errors, and mistakes and is accepted as partial fulfillment for award of MS/M.Phil degree. It is further certified that necessary amendments as pointed out by GEC members and external examiner of the scholar have also been incorporated in the said thesis.


Signature:  \_\_\_\_\_

Name of Supervisor: Dr. Saadi Ishaq \_\_\_\_\_

Date: 20/05/24 \_\_\_\_\_

Signature (HoD):  \_\_\_\_\_

Date: 21-05-2024 \_\_\_\_\_

Signature (Dean/Principal):  \_\_\_\_\_

Date: 23.5.2024 \_\_\_\_\_

**National University of Sciences & Technology****MS THESIS WORK**

We hereby recommend that the dissertation prepared under our supervision by: Waqar Ahmad, Regn No. 00000365272 Titled: Warm Inflation in Hybrid Model be Accepted in partial fulfillment of the requirements for the award of **MS** degree.

**Examination Committee Members**1. Name: DR. MUHAMMAD ALI PARACHA

Signature: \_\_\_\_\_

2. Name: DR. FASIAL MUNIR BHUTTA

Signature: \_\_\_\_\_

Supervisor's Name DR. SAADI ISHAQ

Signature: \_\_\_\_\_

Head of Department

21-05-2024

Date

**COUNTERSIGNED**Date: 23/5/2024

Dean/Principal

## DEDICATION

I extend my deepest gratitude to my teachers, whose guidance and wisdom have been invaluable. To my family and friends, your unwavering support has been my foundation, fueling my determination to excel in this academic pursuit.

## ACKNOWLEDGEMENTS

In writing this Master's thesis, I am indebted to numerous individuals whose support and guidance have been instrumental in its completion. First and foremost, I express my profound gratitude to my thesis supervisor, whose expertise, encouragement, and patience have been invaluable throughout this journey. I also extend my appreciation to Dr. Waqas Ahmed and Dr. M. Junaid for their valuable insights and constructive criticism. Lastly, I am grateful to my family for their unwavering encouragement and understanding, providing me with the necessary strength.

# Contents

<b>LIST OF TABLES</b>	<b>V</b>
<b>LIST OF FIGURES</b>	<b>VI</b>
<b>ABSTRACT</b>	<b>VII</b>
<b>1 Introduction and Motivation</b>	<b>1</b>
<b>2 Cosmology and The Big Bang Model</b>	<b>4</b>
2.1 The Principle of Cosmology . . . . .	4
2.2 The Einstein Field Equations . . . . .	5
2.3 The Friedman Equations . . . . .	6
2.4 Limitations of standard Big Bang Model . . . . .	8
2.4.1 The Horizon Problem . . . . .	9
2.4.2 The Flatness Problem . . . . .	12
<b>3 The Inflation Theory</b>	<b>14</b>
3.1 Solutions Proposed by Inflation . . . . .	16
3.1.1 For the Horizon Problem . . . . .	16
3.1.2 For the Flatness Problem . . . . .	17
3.2 Kinematics of the Inflation Theory . . . . .	17
3.3 Dual Manifestations of Inflationary Dynamics . . . . .	19
3.3.1 Cold Inflation . . . . .	19
3.3.2 Warm Inflation . . . . .	21
3.4 Inflation Observables . . . . .	23
3.4.1 Planck Constraints . . . . .	27
<b>4 Dynamic Equations in Warm Inflation</b>	<b>29</b>
4.1 Warm Inflation Observables . . . . .	30

<b>5</b>	<b>The Principles of Hybrid Inflation</b>	<b>32</b>
5.1	Quantitative Analysis . . . . .	34
<b>6</b>	<b>Conclusion</b>	<b>43</b>
<b>A</b>	<b>Dynamics of the Warm Inflation</b>	<b>45</b>
<b>B</b>	<b>Equations of Motion for Warm Inflation</b>	<b>48</b>



# List of Tables

2.1	Potential scenarios for the evolution of a flat universe ( $k = 0$ ) . . . . .	8
2.2	Evolutionary scenarios for a flattened universe ( $k = 0$ ) . . . . .	12

# List of Figures

2.1	This explains the horizon problem. At the time of reheating, $\tau = 0$ , the regions of spacetime are causally disconnected which raises the horizon problem. Inflation provides a solution to this problem as we can see that these regions are causally connected during the inflationary phase. . . .	9
2.2	Light cone explaining the causality: when the FRW metric is zero, $ds^2 = 0$ , the photon travels along the world line with zero proper time. This is known as the null geodesics. For FRW metric greater than zero, $ds^2 > 0$ , the particle travels with the proper time known as timeline geodesics. Lastly, for $ds^2 < 0$ , the particles are in a causally disconnected spacetime region known as the spacelike interval. . . . .	11
5.1	$n_s$ vs $r$ for linear and quadratic potential with color-coded $\text{Log}(Q)$ . While in the two graphs, $N$ is also taken as fixed i.e. $N = 65$ . . . . .	35
5.2	$Q$ dependence on $V_0$ , $A$ , and $m$ with fixed $N = 65$ and color-coded $n_s$ ranging from 0.90 – 0.97 for linear potential. . . . .	36
5.3	$Q$ dependence on $V_0$ , $A$ , and $m$ with fixed $n_s$ and color-coded $N$ for linear potential. . . . .	37
5.4	$Q$ dependence on $V_0$ , $A$ , and $m$ with fixed $N = 65$ and color-coded $n_s$ ranging from 0.90 – 0.97 for quadratic potential. . . . .	39
5.5	$Q$ dependence on $V_0$ , $A$ , and $m$ with fixed $n_s$ and color-coded $N$ for quadratic potential. . . . .	40
5.6	$n_s$ vs $Q$ for Linear and Quadratic potential with color-coded $V_0$ and fixed $N$ . . . . .	41

# Abstract

Warm inflation describes a scenario in the early universe where inflation occurs with significant thermal interactions, leading to a sustained thermal bath that affects inflation dynamics and subsequent reheating processes. Although we use different models in warm inflation, the hybrid model stands out as fascinating because it incorporates different frameworks of high-energy physics such as SUSY, super-gravity, and GUT. Therefore it is instructive to explore warm inflation in the hybrid model. For this, we present a comprehensive study of warm inflation within the framework of hybrid inflation in a non-supersymmetric model with chaotic potential  $\lambda_p \phi^p$ , incorporating one-loop radiative corrections  $A\phi^4 \ln(\phi/\phi_c)$  where  $A < 0$ . We incorporate quantum smearing effects to investigate the consistency of resulting cosmological observables with Planck and future experiments.

# Chapter 1

## Introduction and Motivation

The Big Bang model serves as a framework for describing the universe's expansion. According to this model, the expansion of the universe states that it was hotter and denser in earlier times which depicts that the universe was radiation-dominated.

Among the most noteworthy accomplishments of this model is the identification of Cosmic Microwave Background (CMB). Multiple space missions such as COBE, WMAP, and the Planck satellite have supported and confirmed this groundbreaking discovery. The obtained measurements disclose an exceptionally close-to-perfect blackbody spectrum, characterized by a temperature of  $T_0 = 2.725K$ . This result is in excellent agreement with the indications made by this model [1].

Extensive testing has been conducted on the concept that at the beginning of the universe, it existed in a more compact and hotter state particularly focusing on the process of Big Bang nucleosynthesis (BBN) which elucidates the synthesis of light elements, comprising hydrogen and its isotopes, helium, and lithium. The abundances of elements have been calculated and compared with observations. These calculations are in excellent agreement with the recorded proportions of these elements in the cosmos. For example, helium constitutes approximately 25% of the matter in the universe which aligns with the projections of the Hot Big Bang framework[5]. Similarly, the observed abundance ratio of deuterium to hydrogen, which is around 1/50,000 aligns with the expectations of the model.

The conventional Big Bang model, broadly embraced in modern cosmology, provides a sound and well-established framework for analyzing the complex and fascinating evolution of the universe over time. This extensively tested model provides a comprehensive explanation of the universe's history, expansion, and CMB radiation. It precisely details the process behind the production of light elements through nucleosynthesis.

While successful in many aspects, this model does possess inherent limitations. The model falls short of providing a complete explanation for certain observed phenomena, notably the high degrees of spatial flatness, homogeneity, and isotropy evident in the universe at a large scale. Nevertheless, the existence of these "problems" does not

imply an inherent disparity within the model. Rather than indicating a fundamental contradiction in the model, these "problems" suggest potential incompleteness, leaving room for the exploration of hidden dynamical mechanisms responsible for these distinctive features.

The most well-elaborated explanation for these phenomena at a large scale in our universe is the theory of inflation. It provides a procedure that helps with the formation of large-scale structures. Inflationary dynamics revolve around the development of inflation, a scalar field, whose potential propels a swift evolution of the cosmos around  $10^{-34}$  seconds following the Big Bang [11]. The theory of inflation is significantly supported by the latest observations of CMB by the Planck satellite [1]. These measurements, which achieved unprecedented accuracy, detected small perturbations in the density at the beginning of the universe. Amplified by gravitational clustering, these density fluctuations eventually start the creation of the observed macroscopic formations in the universe.

This theory encompasses two different types of inflation models. One is cold inflation and the other is warm inflation. The inflaton is considered a distinct system in the framework of cold inflation. The consideration of the relation of the inflaton with other fields occurs exclusively in the computation of radiative corrections to the potential of that scalar field. In this scenario, any additional initial energy density component undergoes red-shifting, resulting in a super-cooled state of the universe. Reheating becomes necessary after inflation ends to transition the cosmos into a phase of radiation-dominated expansion.

Within the cold inflation paradigm, the inflaton field is pivotal in steering the exponential evolution of the universe. Other fields and their interactions have a minor role amid the inflationary phase. While the inflaton field gradually descends along its potential, the universe undergoes rapid expansion, resolving various cosmological problems. Once inflation concludes, the universe remains super-cooled, devoid of thermal equilibrium. Following the conclusion of cold inflation, a reheating phase becomes significant to convert the inflaton field energy into radiation. Reheating marks the transition from the inflationary epoch to a period dominated by radiation. During reheating, the inflaton field decays and produces energetic particles, filling the universe with radiation which ultimately triggers the hot Big Bang phase.

Conversely, warm inflation considers a scenario where the inflaton field is not completely decoupled from other fields during the inflationary period. The relation of the inflaton with the additional fields leads to energy transfer and dissipation, resulting in a non-negligible radiation component during inflation. Warm inflation can alleviate some of the issues associated with cold inflation, such as the formation of primordial density perturbations.

Warm inflation[6, 8] is a realization of inflation in which the relation between inflaton field and other scalar fields plays a crucial role. Besides radiative corrections, these interactions also give rise to the dissipation of energy from the inflaton into various

additional dynamic degrees of freedom. The dissipation takes place resulting in the instability of fields connected to the inflaton, causing it to undergo decay into lighter degrees of freedom. Consequently, these decay processes facilitate the energy transfer from the inflaton to the lighter sector. This process simultaneously dampens the motion of the inflaton field and facilitates particle production, resulting in the creation of a thermal radiation bath. The dissipation of inflaton energy in warm inflation has two significant effects. Firstly, it dampens the movement of the inflaton field, inducing a deceleration. This damping arises from the transfer of energy to the degrees of freedom in the light sector. Secondly, this dissipation process leads to the production of particles in the light sector. These particles can emerge from the decay of the fields that are linked to the inflaton. The production of particles adds to the thermalization of the universe and contributes to the development of a thermal radiation bath.

This thesis centers around the development of the hybrid model that describes inflation in the warm regime. This model aims to incorporate the interactions and dissipation of inflaton energy in a consistent framework. By studying this aspect of warm inflation, researchers can acquire an understanding of the dynamics and phenomenology of the early universe.

# Chapter 2

## Cosmology and The Big Bang Model

One of the pivotal revelations in our comprehension of the universe is the observation that, with the exception of a few nearby galaxies, the majority are receding from us. The rate at which these galaxies move away, indicated by their redshift, intensifies as the distance between us and the galaxies increases. Based on these fundamental observations, we deduce that the universe is a dynamic system in evolution that continuously expands as clusters of galaxies progressively move apart. This chapter provides a comprehensive summary of the foundational principles of the standard cosmology model, establishing a framework for comprehending how the cosmos has evolved. The widely accepted standard Big Bang theory has been extensively reviewed, and interested readers are encouraged to explore these references[4, 13].

### 2.1 The Principle of Cosmology

At the heart of modern cosmology lies the fundamental principle of cosmic evolution. In the framework of this principle, no observer can claim a fixed position within the universe. It postulates the universe's dual characteristics of homogeneity and isotropy. The Friedmann-Robertson-Walker (FRW) metric serves as the mathematical formulation capturing the universe's homogeneity and isotropic nature on large scales:

$$ds^2 = -dt^2 + \frac{a^2(t)dr^2}{1 - kr^2} + a^2(t)r^2 d\theta^2 + a^2(t)r^2 \sin^2(\theta)d\phi^2 \quad (2.1)$$

Here,  $t$  is the cosmic time and the spatial dimensions are parameterized by spherical-polar coordinates  $(r, \theta, \phi)$ . The scale  $a(t)$ , a function of cosmic time, encodes the dynamic nature of the universe i.e. the expansion and contraction. Where  $k$  is the curvature parameter that signifies the types of hypersurfaces:

- $k = +1$  for hypersurfaces characterized by positive curvature,

- $k = 0$  for flat hypersurfaces, and
- $k = -1$  for hypersurfaces characterized by negative curvature.

The FRW (Friedmann-Robertson-Walker) metric elucidates spatial separations regarding comoving coordinates, providing a framework to comprehend spatial dimensions within the context of the expanding or contracting universe. The expansion rate is a crucial parameter that characterizes the FRW spacetime:

$$H(t) = \frac{1}{a(t)} \frac{da}{dt} \quad (2.2)$$

$H(t)$  represents the Hubble parameter which has dimensions of inverse time. Its value can be positive and negative for expansion and contraction of the universe, respectively.

## 2.2 The Einstein Field Equations

The dynamic nature of our universe can be comprehended by employing Einstein's theory proposed in General Relativity, where a connection is developed between matter and geometry of the universe:

$$G_{\mu\nu} + g_{\mu\nu}\Lambda = R_{\mu\nu} - g_{\mu\nu} \left( \frac{1}{2}R - \Lambda \right) = \frac{8\pi G}{c^4} T_{\mu\nu} \quad (2.3)$$

Here  $G_{\mu\nu}$  is the Einstein tensor,  $g_{\mu\nu}$  is the metric tensor,  $\Lambda$  is the cosmological constant,  $R_{\mu\nu}$  is the Ricci curvature tensor,  $R$  is the scalar curvature,  $G$  is the gravitational constant, and  $T_{\mu\nu}$  is the stress-energy tensor representing the distribution of matter and energy.  $G_{\mu\nu}$  is elaborated by Ricci Tensor and Ricci scalar:

$$R_{\mu\nu} = \partial_\alpha \Gamma_{\mu\nu}^\alpha - \partial_\nu \Gamma_{\mu\alpha}^\alpha + \Gamma_{\beta\alpha}^\alpha \Gamma_{\mu\nu}^\beta - \Gamma_{\beta\nu}^\alpha \Gamma_{\mu\alpha}^\beta \quad (2.4)$$

$$R = g^{\mu\nu} R_{\mu\nu} \quad (2.5)$$

The Ricci tensor  $R_{\mu\nu}$ , which characterizes the curvature in the space-time fabric, is developed by combining derivatives of  $g_{\mu\nu}$  expressed as the Christoffel symbols:

$$\Gamma_{\mu\nu}^\alpha = \frac{1}{2} g^{\alpha\beta} \left( \frac{\partial g_{\beta\mu}}{\partial x^\nu} + \frac{\partial g_{\beta\nu}}{\partial x^\mu} - \frac{\partial g_{\mu\nu}}{\partial x^\beta} \right) \quad (2.6)$$

It's crucial to emphasize that the Einstein equations can be conceptualized as a system of equations that establish relationships among tensors. In this particular case, the tensors are  $4 \times 4$  matrices, resulting in a total of 16 distinct equations.



## 2.3 The Friedman Equations

Two fundamental quantities characterize the matter present in the universe at the beginning. These quantities are known as energy density ( $\rho$ ) and pressure ( $p$ ). The Einstein field equations, which can be represented by the Eq. (2.3), explain how gravity works in our universe. The equations propose that gravity is caused by the presence of matter, which deforms the spatial configuration of the cosmos. This deformation is articulated using the metric tensor ( $g_{\mu\nu}$ ), while the energy and momentum of matter are represented by the energy-momentum tensor ( $T_{\mu\nu}$ ). Considering a group of observers whose worldlines align with the timelike 4-velocity,  $u^\mu$  is:

$$u^\mu = \frac{dx^\mu}{d\tau} \quad (2.7)$$

Considering the observers following proper time ( $\tau$ ), the equation  $g_{\mu\nu}u^\mu u^\nu = -1$  holds. The universe's expansion can be approximated by perfect fluids that are homogeneous, isotropic, and exhibit no heat conduction or viscosity. The characterization of these fluids involves specifying their energy density ( $\rho$ ) and pressure ( $p$ ). In the rest frame, the perfect fluids are "isotropic," resulting in a diagonal form for  $T_{\mu\nu}$  with no net momentum flux in any orthogonal direction. The expression for  $T_{\mu\nu}$  of a perfect fluid involves specifying the values of  $\rho$  and  $p$ :

$$T_\nu^\mu = g^{\mu\alpha}T_{\alpha\nu} = (p + \rho)u^\mu u_\nu - p\delta_\nu^\mu \quad (2.8)$$

In a reference frame comoving with the fluid, the 4-velocity can be characterized as  $u^\mu = (1, 0, 0, 0)$ . This choice of 4-velocity leads to the stress-energy tensor as:

$$T_\nu^\mu = \begin{pmatrix} \rho & 0 & 0 & 0 \\ 0 & -p & 0 & 0 \\ 0 & 0 & -p & 0 \\ 0 & 0 & 0 & -p \end{pmatrix} \quad (2.9)$$

This tensor in Eq. (2.9) allows for the simplification of the Einstein field equations into a system of two interconnected differential equations, often referred to as the Friedmann equations:

$$H^2 = \left(\frac{\dot{a}}{a}\right)^2 = \frac{8\pi G}{3}\rho - \frac{k}{a^2} \quad (2.10)$$

The acceleration equation which is also stated as the Raychaudhuri equation:

$$H^2 + \dot{H} = \frac{\ddot{a}}{a} = -\frac{4\pi G}{3}(3p + \rho) \quad (2.11)$$

In an expanding universe containing ordinary matter, where the dots represent derivatives w.r.t time, it is observed that  $\dot{a} > 0$  (indicating an increasing scale factor) and  $\rho + 3p \geq 0$ . This implies  $\ddot{a} < 0$ , indicating a decelerating expansion. It can be deduced from the observation of the universe's expansion that the scale factor was very small at earlier times whereas it rises over time. Assuming that general relativity and the Friedmann equations hold at very high energy scales, this implies the existence of a fundamental singularity at a specific point in the past when  $a(t) = 0$  while  $t \equiv 0$ . The continuity equation can be derived by using Eq. (2.10):

$$\frac{d\rho}{dt} + 3H(p + \rho) = 0 \quad (2.12)$$

Introducing the equation for state parameter as  $w \equiv \frac{p}{\rho}$ , the continuity equation can be further simplified, resulting in:

$$\rho \propto a^{-3(1+w)} \quad (2.13)$$

By combining this expression with Eq. (2.10), the scale factor ( $a(t)$ ) evolution to time can be derived:

$$a(t) \propto \begin{cases} t^{\frac{2(1+w)}{3}}, & \text{if } w \neq -1 \\ e^{Ht}, & \text{if } w = -1 \end{cases} \quad (2.14)$$

In a flat universe (with  $k = 0$ ), the scale factor  $a(t)$  evolution can take three distinct forms based on the matter and radiation content:

1. For a universe primarily composed of non-relativistic matter ( $w = 0$ ), the scale factor changes over time as  $a(t) \propto t^{2/3}$ .

2. For a universe dominated by radiations ( $w = \frac{1}{3}$ ), the scale factor changes as  $a(t) \propto t^{1/2}$ .

3. For a cosmological constant scenario ( $w = -1$ ), the scale factor changes exponentially as  $a(t) \propto e^{Ht}$ .

In a universe composed of diverse matter types like baryons, photons, dark matter, and neutrinos, the characterization of  $\rho$  and pressure  $p$  involves summing the individual contributions. This allows us to express them as:

$$\rho = \sum_i \rho_i, \quad p = \sum_i p_i, \quad w_i = \frac{p_i}{\rho_i} \quad (2.15)$$

The present energy density ratio is described as the quotient of the current energy density to the critical energy density.

$$\Omega_i \equiv \frac{\rho_i}{\rho_c} \quad (2.16)$$

Matter Component	Equation of State	$a(t)$
Matter Dominated	$w = 0$	$a(t) \propto t^{\frac{2}{3}}$
Radiation Dominated	$w = \frac{1}{3}$	$a(t) \propto t^{\frac{1}{2}}$
Cosmological Constant	$w = -1$	$a(t) \propto e^{Ht}$

**Table 2.1.** Potential scenarios for the evolution of a flat universe ( $k = 0$ )

In this expression,  $\rho_i$  represents the energy density of the matter species 'i', and  $\rho_c$  is the critical energy density given by  $\rho_c = 3H_0^2/8\pi G$ . Where subscript '0' in  $H_0$  denotes the quantity at present, normalizing the scale factor to the present time ( $a_0 = a(t_0) \equiv 1$ ) can reformulate Eq. (2.10) as follows:

$$\left(\frac{H}{H_0}\right)^2 = \frac{\Omega_k}{a^2} + \sum_i \frac{\Omega_i}{a^{3(1+w_i)}} \quad (2.17)$$

The curvature parameter  $\Omega_k$  is defined as  $\Omega_k \equiv -k/a_0^2 H_0^2$ , where  $k$  is the curvature constant,  $a_0$  is the current value of the scale factor, and  $H_0$  is the value of the Hubble parameter at present. At present, we derived the formula:

$$\sum_i \Omega_i + \Omega_k = 1 \quad (2.18)$$

Assessing the Eq. (2.11) at the current epoch results in:

$$\frac{1}{a_0 H_0^2} \frac{d^2 a_0}{dt^2} = -\frac{1}{2} \sum_i \Omega_i (1 + 3w_i) \quad (2.19)$$

This equation summarizes the dynamics of the universe's expansion, linking the acceleration of the scale factor to the contributions from various components of the universe, each characterized by its density parameter and equation of state.

## 2.4 Limitations of standard Big Bang Model

As discussed in Chapter 1, the Big Bang model does possess limitations. The model falls short of providing a complete explanation for certain observed phenomena i.e. spatial flatness, homogeneity, and isotropy evident in the universe at a large scale. We will discuss these problems in detail here.

### 2.4.1 The Horizon Problem

Within this model, the position and velocity of every particle in the universe are defined on a spatial slice (3-surface) with time taken as constant. This spatial slice is denoted as  $\Sigma$ . The system is then dynamically evolved by utilizing the laws of physics.

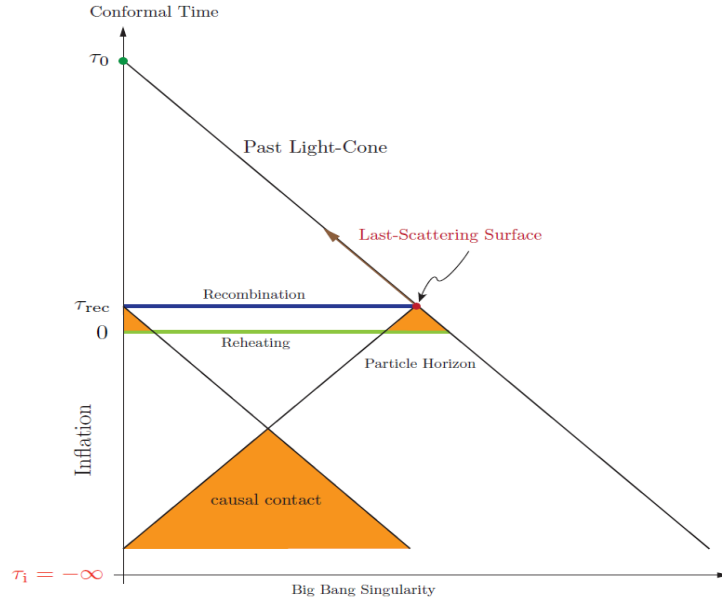


Figure 2.1: This explains the horizon problem. At the time of reheating,  $\tau = 0$ , the regions of spacetime are causally disconnected which raises the horizon problem. Inflation provides a solution to this problem as we can see that these regions are causally connected during the inflationary phase.

The density ( $\rho$ ) and pressure ( $p$ ) characterize the spatial distribution of matter. Gravitationally, inhomogeneities in the distribution are inherently unstable, resulting in their gradual enlargement. This suggests that much more compact small-scale anomalies might have existed in the past in comparison to the current cosmos. The question arises as to how the initial smoothness or homogeneity of the universe can be understood. In the initial phases of the Big Bang model, various regions of space were causally disconnected within the universe. However, during our observation of these regions in the present time, they appeared to exhibit remarkably similar physical properties. This made us think about how these causally disconnected regions evolved to exhibit such similarity. The issue of this initial homogeneity is considered as the horizon problem which can be addressed by considering the propagation of photons in the FRW spacetime.

## Conformal Time, Geodesics and Horizons

Following null geodesics ( $ds^2 = 0$ ), the formulation of the FRW spacetime structure involves the propagation of light, where massless photons play a crucial role. To further analyze spacetime, it is convenient to use the concept of conformal time.

$$\tau = \int \frac{1}{a(t)} dt \quad (2.20)$$

thus the FRW metric can be modified as follows:

$$ds^2 = -a(\tau)^2 d\tau^2 + \frac{a(\tau)^2 d\chi^2}{1 - k\chi^2} + a(\tau)^2 \Phi_k(\chi)^2 d\theta^2 + a(\tau)^2 \Phi_k(\chi)^2 \sin^2(\theta) d\phi^2 \quad (2.21)$$

where,

$$r^2 = \Phi_k(\chi^2) \equiv \begin{cases} \sin^2(\chi) & \text{for } k = 1 \\ \chi^2 & \text{for } k = 0 \\ \sinh^2(\chi) & \text{for } k = -1 \end{cases} \quad (2.22)$$

Given the isotropy of the universe, the formulation for the FRW metric can be made simpler by assuming radial light propagation through the two-dimensional line element:

$$ds^2 = -a(\tau)^2 d\tau^2 + a(\tau)^2 d\chi^2 \quad (2.23)$$

This form of FRW metric can deduce that the radial null-geodesics of light will entertain

$$\chi(\tau) = \pm\tau + \text{constant} \quad (2.24)$$

in conformal time. This means that light will follow a straight line path at an angle of  $45^\circ$ , in the  $\tau - \chi$  plane. The comoving particle horizon, representing the maximal distance a particle travels from an initial time  $t_i$  to a later time  $t_f$ , is denoted as:

$$\chi(\tau) = \tau - \tau_i = \int_{t_i}^{t_f} \frac{1}{a(t)} dt \quad (2.25)$$

Here,  $\tau_i$  represents the initial conformal time. If  $t_i$  is representing the time when the first singularity occurred, denoted as  $t_i = 0$  with  $a = 0$ , a relationship can be established between the comoving and the physical particle horizon using the scale factor.

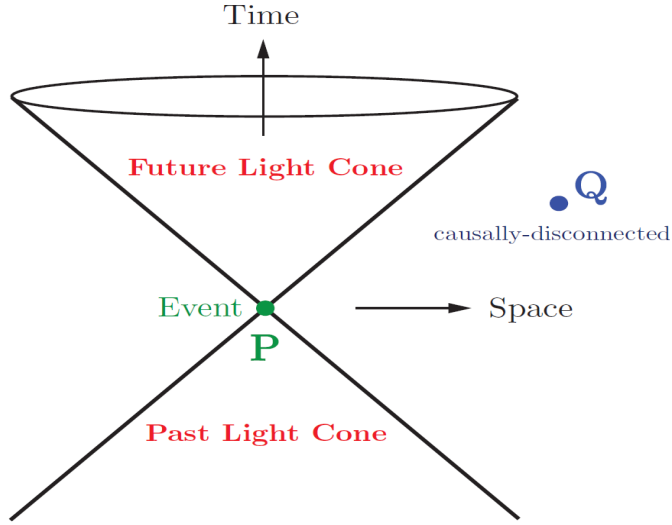


Figure 2.2: Light cone explaining the causality: when the FRW metric is zero,  $ds^2 = 0$ , the photon travels along the world line with zero proper time. This is known as the null geodesics. For FRW metric greater than zero,  $ds^2 > 0$ , the particle travels with the proper time known as timeline geodesics. Lastly, for  $ds^2 < 0$ , the particles are in a causally disconnected spacetime region known as the spacelike interval.

$$d_e(t) = a(t) \cdot \chi_{\text{event horizon}} \quad (2.26)$$

The greatest distance that light may travel from the beginning time  $t_i = 0$  to the final time  $t_f = t$  is represented by the comoving particle horizon. It is provided by:

$$\tau \equiv \int_0^t (a(t'))^{-1} dt' = \int_0^a (Ha^2)^{-1} da = \int_0^a (aH)^{-1} d \ln a \quad (2.27)$$

In the scenario where the universe appears to be predominantly influenced by a fluid characterized by a state equation  $\omega$ , the comoving Hubble radius,  $(aH)^{-1}$ , can be expressed as:

$$(aH)^{-1} = \frac{1}{H_0} a^{\frac{1+3w}{2}} \quad (2.28)$$

The trajectory of the comoving Hubble radius is determined by the sign of  $\omega$ , whether it is positive or negative. Specifically, in cases where either radiation or matter dominates the cosmos. In this case,  $\tau$  is relative to:

$$\tau = \int_0^a \frac{da}{Ha^2} \propto \begin{cases} a, & \text{for RD,} \\ a^{1/2}, & \text{for MD.} \end{cases} \quad (2.29)$$

The development of the comoving horizon with time is monotonous, taking into account the comoving scales currently entering the horizon, it's important to note that the decoupling period was when these scales were first outside the horizon. Despite this, the uniformity seen in the CMB suggests a cosmos that was extraordinarily uniform when the last scattering occurred, extending across large expanses of space that were causally unconnected.

Dominant Component	$w$	$\rho(a)$	$a(t)$	$a(\tau)$	$\tau_i$
Radiation-Dominated (RD)	$\frac{1}{3}$	$a^{-4}$	$t^{1/2}$	$\tau$	0
Matter-Dominated (MD)	0	$a^{-3}$	$t^{2/3}$	$\tau^2$	0
Cosmological Constant ( $\Lambda$ )	-1	$a^0$	$e^{Ht}$	$-\tau^{-1}$	$-\infty$

**Table 2.2.** Evolutionary scenarios for a flattened universe ( $k = 0$ )

## 2.4.2 The Flatness Problem

This cosmological problem becomes apparent when the current energy density of the universe closely approaches its critical value, represented as  $\rho_c$ . For the universe to evolve in the direction of higher levels of homogeneity over time, the initial velocity of the cosmic fluid must have precise values. If the initial velocity is too high, the expansion occurs too fast which might end with the universe being nearly empty. On the other hand, if the initial velocity is too low, the universe collapses. Taking into account the horizon problem as well, this implies that the initial fluid velocity needs to be calibrated over causally disconnected regions. This initial velocity calibration is commonly known as the flatness problem. Remarkably, the universe is nearly a flat Euclidean space, given that the matter within it influences the dynamic nature of spacetime as described by the Einstein field equations. Consider the ratio of densities to be:

$$\Omega(a) \equiv \rho(a)/\rho_c(a) \quad (2.30)$$

Where critical density can be expressed as follows:

$$\rho_c(a) \equiv \frac{3H(a)^2}{8\pi G} \quad (2.31)$$

We can modify the Eq. (2.10) as:

$$1 - \Omega(a) = \frac{-k}{(aH)^2} \quad (2.32)$$

In relation to the conventional Big Bang theory, the density parameter  $\Omega(a)$  is time-dependent, and the Hubble radius  $(aH)^{-1}$  increases as time passes. As a consequence, the absolute value of  $\Omega - 1$  diverges w.r.t time, and the critical value  $\Omega = 1$  becomes an unstable fixed point. Hence, the current value  $|\Omega(a_0)| \approx 1$  needs a highly fine-tuned initial value at the beginning of the universe. Furthermore, variations from flatness throughout major epochs including the Planck scale, the Grand Unified Theory period, and BBN have been shown to need upholding certain requirements [4]:

$$\begin{aligned} |\Omega(a_{\text{Planck}}) - 1| &\leq O(10^{-61}) \\ |\Omega(a_{\text{GUT}}) - 1| &\leq O(10^{-55}) \\ |\Omega(a_{\text{BBN}}) - 1| &\leq O(10^{-16}) \end{aligned}$$

By utilizing the continuity equation after differentiating the Friedmann equation, we obtain the following expression:

$$\frac{1}{\Omega(\Omega - 1)} \frac{d\Omega}{d \ln a} = (1 + 3w) \quad (2.33)$$

From the derived inequality,  $1 + 3w > 0$ , it can be concluded that  $\Omega = 1$  is an unstable fixed point. This implies that any fluctuation in the density parameter  $\Omega$  from singularity will lead to a divergence from  $\Omega = 1$  instead of convergence towards it.

$$\frac{d|\Omega - 1|}{d \ln a} > 0 \Rightarrow 1 + 3w > 0 \quad (2.34)$$

The existence of these problems within the standard cosmological model does not indicate an inherent inconsistency in the model itself but rather suggests that the model may be incomplete and lack a fundamental dynamical mechanism to account for these particular attributes. The anticipation of the universe's homogeneity and flatness cannot be inherently derived from this model alone. Instead, these features must also be regarded as fundamental conditions, underscoring a limitation in the predictive capacity of the model. Inflation has become the forefront candidate for explaining the dynamic origins of these fundamental conditions in the cosmos [4].



# Chapter 3

## The Inflation Theory

The cosmological problems discussed in the previous chapter are due to the increasing comoving Hubble radius  $(aH)^{-1}$ . However, inflation serves as a solution to these challenges which is thoroughly examined and widely acknowledged in [4, 8, 13], and stands as well a well-established theory for various aspects of the visible universe, encompassing both homogeneities at large-scale and spatial flatness. Additionally, this theory also ensures that the comoving Hubble radius decreases at the very early universe ( $10^{-36} - 10^{-34}s$ ) [11], i.e.

$$\frac{d(aH)^{-1}}{dt} < 0 \quad (3.1)$$

In the light of Eq.(2.11), it is straightforward to find

$$\frac{d^2 a}{dt^2} > 0 \quad (3.2)$$

provided that

$$\rho + 3p < 0 \quad (3.3)$$

Consequently, space will undergo an accelerated expansion that leads to homogeneity at a large scale and spatially flat universe. From Eq.(2.11), one can easily deduced

$$\frac{\ddot{a}}{a} = H^2(1 - \epsilon) \quad (3.4)$$

where  $\epsilon$  is a slow-roll parameter and is defined as:

$$\epsilon \equiv \frac{-\dot{H}}{H} \quad (3.5)$$

One can deduce that an epoch of accelerated evolution is possible whenever this  $\epsilon$

satisfies this condition:  $\epsilon < 1$ . We can also write  $\epsilon$  in terms of the number of e-folds ( $N_e$ ):

$$\epsilon \equiv -\frac{\dot{H}}{H^2} = -\frac{d \ln H}{dN_e} < 1 \quad (3.6)$$

## Number of e-folds

The logarithmic expansion factor of  $a(t)$  during accelerated expansion is expressed as the number of e-folds ( $N_e$ ).

$$N_e = \log \left( \frac{a_e}{a_i} \right) \quad (3.7)$$

where  $a_i$  and  $a_e$  represent the scale factors at the start and end of the inflationary period. This parameter provides a measure of the total expansion that happened in this period of inflation. One can calculate this parameter through Eq. (3.7):

$$N_e(\phi) = \int_{t_{end}}^t H dt = \int_{\phi_{end}}^{\phi} H(\dot{\phi})^{-1} d\phi \approx \int_{\phi}^{\phi_{end}} V(V,\phi)^{-1} d\phi \quad (3.8)$$

This expression can be adjusted in the context of slow-roll parameters as:

$$N_e(\phi) = \int_{\phi}^{\phi_{end}} (2\epsilon)^{-\frac{1}{2}} d\phi \quad (3.9)$$

To address the cosmological problems, a sufficient amount of inflation is required, typically around 50-60 e-folds. Mathematically, this can be expressed as:

$$e^{N_e} = \frac{a_{end}}{a_{start}} \approx 50 - 60 \quad (3.10)$$

This condition ensures that the universe undergoes an enough long phase of accelerated expansion, allowing for the settlement of these cosmological problems. For the accelerated expansion, Eq. (2.10) can also be used to extract the conditions on energy density and pressure of the universe:

$$\frac{d(aH)^{-1}}{dt} < 0 \Rightarrow \ddot{a} > 0 \Rightarrow 3p + \rho < 0 \quad (3.11)$$

This implies that the energy density and pressure of the universe must satisfy the following condition for an accelerated expansion:

$$p < -\frac{1}{3}\rho \quad (3.12)$$

Based on this condition, it can be asserted that any duration of expansion during the inflation will feature a contracting Hubble sphere, distinguished by a decreasing comoving Hubble radius. This leads to accelerated expansion, where the scale factor of the universe rises rapidly. Additionally, inflation is associated with a negative pressure, which contributes to the exponential expansion.

In the context of inflation, the integration of the comoving Hubble radius can give the expression for the conformal time:

$$\tau = \int_0^a (a'H(a'))^{-1} d \ln a' \quad (3.13)$$

In case the  $(aH)^{-1}$  is considerably smaller than the  $\tau$ , it implies that particles outside the current Hubble radius were causally connected at a specific moment at the beginning of the universe. This can only be true if the comoving horizon receives significant contributions from the time of the universe when the Hubble radius was larger. Inflationary expansion can facilitate this scenario as it involves a phase where Hubble's radius decreases. During inflation, the scale factor  $a$  shows an exponential growth but the Hubble parameter  $H$  stays approximately constant.

## 3.1 Solutions Proposed by Inflation

### 3.1.1 For the Horizon Problem

The decrease in the value of the comoving Hubble radius deduces that large-scale structures were causally connected before the inflation. This would enable causal physics to contribute in the development of the universe's homogeneity. A flat FRW spacetime metric is represented as follows::

$$ds^2 = -a(\tau)^2 d\tau^2 + a(\tau)^2 dx^2 \quad (3.14)$$

This metric describes the spatial and temporal structure of the universe. The metric component  $dx^2$  represents the spatial dimensions.

A null geodesic has  $ds^2 = 0$ , and in conformal coordinates, we can express it as  $d\tau = \pm\sqrt{dx^2}$ . For matter and radiation domination, the scale factor changes in the following ways:

$$a(\tau) \propto \begin{cases} \tau^2 & \text{MD} \\ \tau & \text{RD} \end{cases} \quad (3.15)$$

This indicates that the scale factor increases with conformal time, leading to an expanding universe. The specific power-law dependence of  $a(\tau)$  on  $\tau$  depends on the dominant energy component during that epoch.

The horizon problem arises when we consider the causal history of different spacetime points in the universe. The figure (2.1) illustrates that points are causally connected and exhibit intersecting light cones at the initial singularity i.e.  $\tau_i = 0$ . However, at around  $3.8 \times 10^5$  years of age, the decoupling of photons from electrons enables them to move freely with minimal interaction. At this time, known as the last scattering ( $\tau_{\text{CMB}}$ ), the universe comprised several causally disconnected regions that were not in thermal equilibrium. By introducing accelerated expansion, inflation provides a solution to this problem. This nearly exponential expansion during inflation allows causally disconnected regions to connect causally and establish equilibrium thermally.

The Hubble parameter  $H$  is approximately the same throughout inflation. This implies that the scale factor ( $a$ ) approaches 0 in the infinite past, as  $\tau_i \rightarrow -\infty$ . Similarly, the scale factor  $a$  becomes infinite when  $\tau = 0$ , indicating that inflation continues into the never-ending future. However, it should be noted that the expression for the scale factor breaks down after inflation ends.

As a result, the initial singularity returns to an unbounded conformal time,  $\tau \ll 0$ , and the point  $\tau = 0$  now indicates the conclusion of the inflation. Although points in the universe may look causally disconnected, they are causally connected in reality due to the possibility of light cone enlargement during the conformal time from  $\tau = 0$  to  $\tau = -\infty$ .

### 3.1.2 For the Flatness Problem

Inflation also helps us to solve the Flatness problem can also be solved the inflation. Since the density parameter is related to comoving Hubble radius as:

$$\Omega(a) = 1 + \frac{1}{(aH)^2} \quad (3.16)$$

The solution  $\Omega = 1$  is only feasible for the  $(aH)^{-2} \ll 0$ . The inflation explains this decrease in the value of  $aH$ . Eventually, the curvature of the universe will move towards spatial flatness.

## 3.2 Kinematics of the Inflation Theory

Inflation fundamentally relies on achieving an equation of state characterized by negative pressure. This phenomenon can be naturally explained by quantum fields present in the early universe. A crucial insight from quantum field theory is that these fields

can produce an energy density similar to that of a cosmological constant. Here, we will focus on a scalar field, denoted as  $\phi$ , which is generally complex but often exemplified using a single real field for simplicity. This emphasis on scalar fields is not merely for simplicity; it is also due to the relatively unexplored nature of the scalar sector in particle physics. While vector fields like electromagnetism are well understood, many unification theories predict the existence of additional scalar fields, such as the Higgs field. We will now explore the implications of these fields for cosmology.

We propose the implementation of inflation using a single canonical scalar field  $\phi$ , known as the inflaton, governed by a potential  $V(\phi)$ . During inflation, this scalar field slowly rolls towards its minimum, a process described by the slow-roll condition, which has shown great success. Let us now examine in detail how the inflationary phase unfolds.

The vacuum energy density which drives the inflation, has to be a dynamic quantity that evolves with time. This dynamic evolution can be modeled using the inflaton field with the action:

$$S = \int d^4x \left[ \sqrt{-g} \frac{1}{2} R + \sqrt{-g} \left( \frac{1}{2} g^{\mu\nu} \partial_\mu \phi \partial_\nu \phi - V(\phi) \right) \right] = S_{EH} + S_\phi \quad (3.17)$$

Where  $S_{EH}$  represents the Einstein-Hilbert action and  $S_\phi$  represents the canonical kinetic term of the scalar field action. Considering that the scalar field is in a homogenous state,  $\phi(t, x) = \phi(t)$ , the energy-momentum tensor can be formulated as:

$$T_{\mu\nu}^\phi \equiv -\frac{2}{\sqrt{-g}} \frac{\delta S_\phi}{\delta g^{\mu\nu}} = \partial_\mu \phi \partial_\nu \phi - \frac{g_{\mu\nu}}{2} \dot{\phi}^2 + g_{\mu\nu} V(\phi) \quad (3.18)$$

By taking the expression of  $g_{\mu\nu}$  from Eq. (2.1) and using it in Eq. (3.18), we can have the following relations for energy density and pressure:

$$\rho_\phi = \frac{\dot{\phi}^2}{2} + V(\phi) \quad (3.19)$$

$$p_\phi = \frac{\dot{\phi}^2}{2} - V(\phi) \quad (3.20)$$

The state parameter equation,  $w_\phi$ , can be established as the quotient of pressure to energy density:

$$w_\phi = \frac{p_\phi}{\rho_\phi} = \frac{\frac{1}{2} \dot{\phi}^2 - V(\phi)}{\frac{1}{2} \dot{\phi}^2 + V(\phi)} \quad (3.21)$$

For a scalar field, negative pressure ( $w_\phi < 0$ ) and accelerated expansion ( $w_\phi \approx -1/3$ ) can be generated whenever the potential term  $V(\phi)$  is dominating over the kinetic term  $\frac{1}{2}\dot{\phi}^2$ . This implies that the scalar field needs to be "slowly rolling" during inflation.

### 3.3 Dual Manifestations of Inflationary Dynamics

The pursuit of a viable framework that can drive inflation with slow-roll conditions has resulted in two diverse dynamical implementations of inflation. The first is known as cold inflation with interactions between the inflaton and any other field taken into account only for radiative corrections to the scalar potential. The second implementation, known as warm inflation, was initially described in [4, 13]. Warm inflation allows for the simultaneous generation of particles during the inflationary expansion by dissipating inflaton energy through interactions among the inflaton field and other fields. Numerous warm inflation models have been developed since then, spanning a wide range of theoretical proposals [14].

#### 3.3.1 Cold Inflation

Cold inflation, the conventional inflationary scenario, depicts a time in the universe's early history when exponential growth was occurring rapidly. The driving force behind the universe's expansion lies in the potential energy of a scalar field called the inflaton. This phenomenon addresses key cosmological problems and offers a comprehensive solution.

##### Mechanism of Cold Inflation

Cold inflation relies on the inflaton, characterized by a potential energy landscape that influences the early universe's energy density. Undergoing a slow roll along its potential, the inflaton field facilitates a sustained phase of exponential expansion. The conditions for this phase are encapsulated in the slow-roll parameters, which must be small for effective inflation.

The end of inflation occurs as the inflaton reaches the bottom of its potential energy and reheat. Reheating is the process by which the inflaton decays into standard particles as a result of the field's subsequent oscillations around this minimum. This is the point at which the hot Big Bang phase begins[13].

For cold inflation, the equation of motion governing the inflaton field ( $\phi$ ) can be formulated as:

$$\ddot{\phi} + 3H\dot{\phi} + V_{,\phi} = 0 \tag{3.22}$$

Recalling the equation for the reduced Planck mass:

$$m_p = (8\pi G)^{-\frac{1}{2}} \quad (3.23)$$

The pressure ( $p$ ), energy density ( $\rho$ ), and Hubble parameter ( $H$ ) of the scalar field controlled by the Friedmann equations are related in the following way:

$$H^2 = \frac{1}{6m_p^2} \left( \dot{\phi}^2 + 2V(\phi) \right) \quad (3.24)$$

Assuming the homogeneity of a scalar field dominates the universe, the acceleration equation takes on the form:

$$\frac{\ddot{a}}{a} = -\frac{4\pi G}{3}(\rho_\phi + 3p_\phi) = H^2(1 - \epsilon) \quad (3.25)$$

Sustaining a phase of accelerated evolution is dependent on the condition  $\epsilon < 1$ . The de Sitter condition ( $p_\phi \rightarrow -\rho_\phi$ ) provides a means to fulfill the requirement where  $\epsilon \rightarrow 0$  and the potential energy remains dominant over the kinetic energy ( $\dot{\phi}^2 \ll V(\phi)$ ). To ensure successful inflationary cosmology, the second differential of the inflaton field  $\phi$  must be at a minimum during the inflationary epoch. Close monitoring of the inflaton field behavior is crucial to meet this condition and achieve the desired expansion, given by:

$$|\ddot{\phi}| \ll |3H\dot{\phi}|, |V_{,\phi}| \quad (3.26)$$

Introducing a second slow-roll parameter as a consequence of this condition:

$$\eta = -\frac{\ddot{\phi}}{H\dot{\phi}} = \epsilon - \frac{1}{2\epsilon} \frac{d\epsilon}{dN_e} < 1 \quad (3.27)$$

Ensuring the dominance of the potential over kinetic energy and maintaining a modest acceleration of the inflaton field about the Hubble parameter is achieved through these conditions. Therefore, Eq. (3.22) turns to be

$$\dot{\phi} \approx -\frac{V_{,\phi}}{3H} \quad (3.28)$$

and Eq. (3.24) reads as:

$$H^2 \approx \frac{1}{3} \frac{V(\phi)}{m^2} \approx \text{constant} \quad (3.29)$$

The fulfillment of these conditions results in the spacetime approximating a de Sitter space, characterized by the scale factor which can be expressed as:

$$a(t) \sim e^{Ht} \tag{3.30}$$

These equations illustrate the nearly constant value of the Hubble parameter, the inflaton field evolves slowly, and the universe experiences an exponential expansion during inflation.

Expressing the potential-dependent slow-roll parameters in terms of the Hubble slow-roll parameters is also a viable approach:  $\epsilon = \epsilon_\phi$  and  $\eta = \eta_\phi - \epsilon_\phi$ , inflation ends when the slow-roll requirements are not followed,  $\epsilon = \epsilon_\phi \equiv 1$ .

The inflaton field leads to a rapid redshift of other initial components of energy density during this expansion period. Consequently, the universe enters into a supercooled state. After the end of the inflation, a different state, known as reheating, becomes necessary that carry the cosmos into a radiation-dominated period of expansion [6]. It can be attained if the inflaton field undergoes coherent oscillations occurring around the minimal potential, effectively behaving as pressureless matter, when the inflationary era ends. Mathematically, this phenomenon is articulated by the equation:

$$\dot{\bar{\rho}}_\phi + 3H\bar{\rho}_\phi = 0 \tag{3.31}$$

where  $\bar{\rho}_\phi$  represents the average energy density of the inflaton field. Other degrees of freedom must interact with the inflaton field as it decays.

## Predictions and Observations

Cold inflation naturally explains the observed homogeneity and flatness of the universe, as the exponential expansion dilutes any initial curvature and homogenizes the observable universe. The theory predicts an almost scale-invariant spectrum of primordial density variations, closely matching CMB observations and the distribution of galaxies. The universe remains in a super-cooled state during inflation, only reheating after the inflaton decays, transforming potential energy into particles and radiation.

### 3.3.2 Warm Inflation

Warm inflation in cosmology offers a different approach from the cold inflation model. It addresses the same cosmological problems by introducing a mechanism where the universe remains warm due to the continuous development of radiation during inflation. In this approach, the inflaton field engages in interactions with other fields, dissipating



its energy into a thermal bath. This process maintains the temperature of the universe, contrasting with the supercooling that occurs in cold inflation.

### Key Features of Warm Inflation

The inflaton dissipates energy as it rolls down its potential, sustaining the universe's temperature despite the exponential expansion. Particle production occurs throughout the inflationary period, eliminating the need for a distinct reheating phase post-inflation. It generates primordial density fluctuations from both thermal and quantum fluctuations, differing from cold inflation's predominantly quantum origin.

In the most straightforward warm inflation scenario, the particles generated undergo rapid thermalization, surpassing the Hubble expansion rate. This leads to a quasi-adiabatic along with nearly stable evolution, where the main difference occurs in the inflaton field motion equation by the addition of the dissipation coefficient,  $\Gamma$ , which plays the role of friction during inflation. Suppose the generated particles are both light in comparison to the surrounding temperature and exhibit relativistic behavior. In that case, the inflaton field's energy is effectively dissipated into an almost-thermal radiation bath [8]. The background equations for the inflaton field and radiation energy density can be represented as:

$$\ddot{\phi} + \dot{\phi}(\Gamma + 3H) + V_{,\phi} = 0 \quad (3.32)$$

$$\dot{\rho}_R - \Gamma\dot{\phi}^2 + 4H\rho_R = 0 \quad (3.33)$$

The radiation energy density is to be described as:

$$\rho_R = \frac{\pi^2 g_* T^4}{30} \quad (3.34)$$

While  $g_*$  represents the light degrees of freedom. The warm inflation model takes the dissipative ratio into account, denoted by  $Q$  and defined as:

$$Q = \frac{\Gamma}{3H} \quad (3.35)$$

Taking the system into account within the slow-roll regime and  $\ddot{\phi} \ll 1$ , Eq. (3.32) and Eq. (3.33) can be estimated as:

$$(1 + Q)\dot{\phi} \approx \frac{-V_{,\phi}}{3H} \quad (3.36)$$

$$4H\rho_R \approx \Gamma\dot{\phi}^2 \quad (3.37)$$

By introducing the dissipative ratio, the slow-roll conditions will be modified as:

$$\epsilon = \frac{1}{16\pi G(1+Q)} \left( \frac{V_{,\phi}}{V(\phi)} \right)^2 < 1 \quad (3.38)$$

$$|\eta| = \frac{1}{8\pi G(1+Q)} \left| \frac{V_{,\phi\phi}}{V(\phi)} \right| < 1 \quad (3.39)$$

whereas  $V_{,\phi}$  and  $V_{,\phi\phi}$  are the first and second derivatives of the potential w.r.t the inflaton field.

In the warm regime, slow-roll inflation can be sustained for seeing the situations  $\eta, \epsilon < (1+Q)$  permit. When there is a powerful dissipative regime like  $Q$  is greater than unity ( $Q \geq 1$ ), these conditions can hold without any variation in the potential. The following relationship expresses how radiation energy density is subdominant over potential:

$$\frac{\rho_R}{\rho_\phi} \approx \frac{\epsilon}{2Q(1+Q)} \leq 1 \quad (3.40)$$

When the value of  $Q$  becomes large, the system enters a strong dissipative regime. As slow-roll inflation ends at  $\epsilon \approx 1+Q$ , radiation may now contribute a significant amount to the universe's overall energy density. This is due to an increase in radiation energy density in relation to the scalar potential. In the event that inflation ends within the strong dissipative regime such as  $Q$  is significantly greater than unity ( $Q \gg 1$ ), the energy density of the universe sees a rapid transition [8].

### Implications and Predictions

The primordial fluctuation spectrum in warm inflation might present unique features due to the influence of thermal fluctuations. These characteristics could be identified through measurements of the CMB and the universe's large-scale structure. The absence of a separate reheating phase provides a smoother shift of inflation to the conventional hot Big Bang model. Warm inflation's success relies on matching its predictions with accurate measurements of the CMB, large-scale structures, and possibly gravitational waves. Developing a fully consistent model that aligns with all observational data remains a challenge and an active area of research.

## 3.4 Inflation Observables

For a physical theory to be considered successful, it must be in agreement with observations. Observations are pivotal in the field of cosmology, shaping our comprehension of

the universe. As opposed to particle physics, which studies high-energy events through collider experiments, cosmology relies on observations of the universe at large scales. Inflationary cosmology has emerged as a compelling framework that explains several key observations. It naturally accounts for the observed high degree of uniformity and spatial flatness as the cosmos exists right now. The shrinking Hubble radius during inflation also allows for the creation of quantum fluctuations. These fluctuations serve as the first seeds from which the universe's large-scale structures grow. They arise from inhomogeneities in the inflaton field and result in the development of gravitationally unstable density perturbations.

The study of inflationary perturbations has been the subject of extensive research and review, as it provides insights into the origin of cosmic structure and the formation of galaxies and clusters. Notable reviews have delved into the theoretical aspects and observational consequences of inflationary perturbations [10]. These studies bridge the gap between theoretical models and experimental data, helping us develop a more comprehensive understanding of the beginning of the universe.

Since the inflaton is a quantum field, there are variations in its behavior. Heisenberg's uncertainty principle states, it is impossible to measure the field's value and associated momentum with absolute certainty. This leads to the expectation that the inflaton field will manifest slight quantum fluctuations surrounding its constant value.

$$\phi(x, t) = \tilde{\phi}(t) + \delta\phi(x, t) \quad (3.41)$$

whereas  $\tilde{\phi}(t)$  complies with the equations of motion of classical systems which are discussed previously and  $\delta\phi$  is much smaller compared to  $\tilde{\phi}(x, t)$ .

Throughout the inflationary epoch,  $H$  remains almost constant, whereas the scale factor  $a(t)$  experiences swift exponential growth, typically increasing by one e-fold within a time frame roughly equivalent to  $H^{-1}$ . On the other side, microphysical processes face constraints in affecting length scales larger than  $O(H^{-1})$ .

Before inflation, for causally connected scales in our universe, we require  $k/aH < 1$ . As inflation proceeds, the Hubble radius reduces, and at a certain stage called "horizon crossing," we have  $k/aH \approx 1$ . After this stage, when  $k/aH > 1$ , microphysical processes are no longer effective, and the perturbations freeze in their evolution. These frozen perturbations behave as classical cosmological perturbations, causing gravitational instabilities that lead to the creation of high-scale structures upon re-entering the horizon at a time when we have  $k/aH > 1$  again. The equation describing the variations in the inflaton field is as follows:

$$\delta\ddot{\phi} + 2aH\delta\dot{\phi} + \frac{k^2}{a^2}\delta\phi = 0 \quad (3.42)$$

whereas  $\delta\phi$  represents the inflaton field fluctuation's amplitude and  $k$  is the comoving wavenumber. The expression for this amplitude is as follows:

$$P_\phi(k) = \frac{H^2}{2k^3} \propto k^{-3} \quad (3.43)$$

Inflation gives rise to quantum fluctuations in the inflaton field, inducing minor inhomogeneities in the underlying spacetime. In the inflationary phase, the energy-momentum tensor experiences similar perturbations when there are changes in the inflaton field. As a result, these perturbations influence the metric of the expanding spacetime, especially at the time when the inflaton field predominantly governs the energy density. These perturbations get expanded and magnified to macroscopic scales as they are frozen over the horizon.

These perturbations also need a more complicated evaluation as compared to fluctuations of an isolated field such as the inflaton. The common approach for investigating metric perturbations involves breaking them down into tensor, vector, and scalar components [12]:

$$ds^2 = g_{\mu\nu}dx^\mu dx^\nu = -(1+2\Phi)dt^2 + 2aB_i dx^i dt + a^2(1-2\Psi)\delta_{ij}dx^i dx^j + a^2 E_{ij}dx^i dx^j \quad (3.44)$$

whereas  $E_{ij}$  represents the tensor quantity,  $B_i$  is defined as a vector quantity, and  $\Phi$  and  $\Psi$  represent the scalar potentials. However, there are not many significant vector perturbations during inflation and decay away, allowing us to neglect them and focus only on the tensor and scalar perturbations.

It is possible to identify the production of scalar perturbations by considering various regions of the universe where the inflaton field may exhibit slightly different values. While these regions undergo the same slow-roll evolution during inflation, the conclusion of inflation will occur at marginally distinct times in each region. Due to this, various regions will undergo a slightly distinct level of expansion.

Following the conclusion of inflation, the energy density becomes distributed, giving rise to fluctuations in the scale factor. This generates curvature and density perturbations. The comoving curvature perturbation that is generated during inflation and remains invariant to gauge is stated as:

$$\mathcal{R} = \Psi - \frac{H}{\rho + p}\delta q \approx \Psi + \frac{H}{\dot{\phi}}\delta\phi \quad (3.45)$$

Here,  $\delta q$  represents the scalar 3-momentum density  $T_i^0 = \partial_i(\delta q)$ .

The comoving curvature perturbation's power spectrum provides information on the link between the curvature of space-time and the division of energy in the cosmos.

The power spectrum describes the fluctuations in density at the beginning of our universe, which is essential in the subsequent formation of galaxies and other large-scale structures, can be represented as:

$$P_{\mathcal{R}}(k) = \left( \frac{H}{\dot{\phi}} \right)^2 P_{\phi} \quad (3.46)$$

A widely accepted practice is to introduce the dimensionless power spectrum  $\Delta_{\mathcal{R}}^2$  that allows for accurate interpretation and understanding of the power spectrum:

$$\Delta_{\mathcal{R}}^2 \equiv \frac{k}{2\pi^2} P_{\mathcal{R}}(k) = \left( \frac{H}{\dot{\phi}} \right)^2 \left( \frac{H}{2\pi} \right)^2 \quad (3.47)$$

It can also be modified as follows:

$$\Delta_{\mathcal{R}}^2 = \frac{1}{24\pi^2} \frac{V}{m_p^4} \frac{1}{\epsilon_{\phi}} \quad (3.48)$$

The scalar spectral index, represented as  $n_s - 1$ , quantifies the deviation of primordial density fluctuations from scale invariance and can be expressed as:

$$n_s = 1 + \frac{d \ln \Delta_{\mathcal{R}}^2}{d \ln k} \quad (3.49)$$

Under the slow-roll approximation, the scalar spectral index can be roughly calculated as:

$$n_s \approx 1 - \frac{m_p^2 V_{,\phi}}{V(\phi)} \frac{1}{\Delta_{\mathcal{R}}^2} \frac{d\Delta_{\mathcal{R}}^2}{d\phi} \quad (3.50)$$

Alternatively, it may be expressed in relation to the slow-roll parameters as follows:

$$n_s \approx 1 + 2\eta_{\phi} - 6\epsilon_{\phi} \quad (3.51)$$

During inflation, tensor perturbations of the metric are created and give rise to primordial gravitational waves. Likewise, there is a connection between scalar perturbations and curvature perturbations. Tensor perturbation power spectrum is expressed as:

$$\Delta_t^2 = \frac{2H^2}{\pi^2 m_p^2} \quad (3.52)$$

Another important observational parameter in the context of inflation is the ratio of tensor to scalar perturbations, denoted as  $r$ . By defining the tensor index as  $n_t = -2\epsilon_\phi$ , we can obtain this ratio:

$$r = 8|n_t| \tag{3.53}$$

Such observations suggest the occurrence of slow-roll inflation within the conventional supercooled domain. However, in the case of warm inflation, the estimations undergo alterations due to the dynamics of fluctuation-dissipation, a subject that will be delved into in the next chapter.

### 3.4.1 Planck Constraints

The early irregularities in the density of the universe, known as primordial density perturbations, are the seeds from which the universe's large-scale structure ultimately emerges. These perturbations also cause the fluctuations observed in the CMB temperature. The data obtained from the Planck satellite observations have been instrumental in constraining inflationary theory.

#### Spectral Index ( $n_s$ )

Planck data has measured the spectral index of CMB fluctuations that is consistent with predictions of simple inflationary models:

$$n_s < 1 \tag{3.54}$$

#### Constraints on Inflation Models

The data from the Planck satellite contributes to narrowing down the set of inflation models that have a closely scale-invariant spectrum of primordial variations.

#### The upper bound for $r$

The inflation energy scale has been limited by the upper limits that Planck observations have imposed on  $r$ :

$$r < 0.058 \tag{3.55}$$

This significantly narrows the parameter space for inflationary theories.

## Non-Gaussianity

Planck has searched for non-Gaussian features in the CMB, with results consistent with Gaussian fluctuations predicted by simple inflationary models, placing tight constraints on any deviations from Gaussianity.

## Implications for Cosmology

The Planck constraints have far-reaching implications for cosmology, including determinations of the universe's age, confirmation of dark matter and dark energy, and refinements in the values of the Hubble constant and other cosmological parameters. The Planck mission's results have significantly constrained the range of parameters viable for inflationary models. The most recent results by Planck satellites are [1]:

$$\Delta_{\mathcal{R}}^2 = 2.2 \times 10^{-9} \quad (3.56)$$

and the constraint on  $n_s$  value has to be:

$$n_s = 0.9665 \pm 0.0038 \quad (3.57)$$

# Chapter 4

## Dynamic Equations in Warm Inflation

The dynamics of warm inflation have undergone extensive review in the literature. The equations of motion along with the observable predictions for warm inflation can be obtained by using the dissipation coefficient  $\Gamma(\phi, T)$  in its functional form. For a detailed derivation, please refer to Appendix A.

The relation that connects the radiation energy density ( $4\rho_R$ ), the dissipative ratio ( $Q$ ), and the inflaton field( $\phi$ ), can be written as  $4\rho_R = 3Q\dot{\phi}^2$  considering the slow-roll conditions to be satisfied. Combining these expressions, we obtain a relationship of  $Q$  with  $\phi$  [3]:

$$Q^{1/3}(1+Q)^2 = 2\epsilon \left(\frac{C}{3}\right)^{1/3} \left(\frac{C}{4C_R}\right) \left(\frac{H}{\phi}\right)^{8/3} \left(\frac{mp}{H}\right)^2 \quad (4.1)$$

where  $C_R = \frac{\rho_R}{T^4} = \frac{\pi^2 g_*}{30}$ . This enables us to obtain motion equations for  $\phi$ ,  $Q$ , and  $T/H$  which represent the ratio of the temperature with  $H$  concerning  $N_e$ . Appendix B gives the detailed derivation of these expressions.

$$\frac{d\phi}{dN_e} = -\frac{\phi}{m_p} \frac{\sigma_\phi}{1+Q} \quad (4.2)$$

$$\frac{dQ}{dN_e} = \frac{Q}{1+7Q} (10\epsilon_\phi - 6\eta_\phi + 8\sigma_\phi) \quad (4.3)$$

$$\frac{d\ln(T/H)}{dN_e} = \frac{2}{(1+q)(1+7Q)} ((2+4Q)\epsilon_\phi - (1+Q)\eta_\phi + (1-Q)\sigma_\phi) \quad (4.4)$$

A new slow-roll parameter is introduced here:

$$\sigma = \frac{m_p^2 V_{,\phi}}{\phi V} \quad (4.5)$$



## 4.1 Warm Inflation Observables

Considering warm inflation, the density perturbation spectrum undergoes modifications due to fluctuation-dissipation effects [4, 7, 8, 13]. This involves the coupling of perturbations in both the radiation fluid and the inflaton, mediated by the  $\Gamma$  that depends on temperature. The perturbations in the inflaton are generated by a Gaussian white noise term  $\zeta_k$ .

$$\ddot{\delta\phi}_k + 3H\dot{\delta\phi}_k + 3HQ\dot{\delta\phi}_k + \frac{k^2}{a^2}\delta\phi_k \approx \sqrt{\frac{2\gamma T}{a^3}}\zeta_k \quad (4.6)$$

where the inflaton's thermal fluctuations are represented by  $\zeta_k$ . It can be estimated by a Gaussian distribution that is localized and has a correlation function [2]:

$$\langle \zeta(t, \mathbf{x})\zeta(t', \mathbf{x}') \rangle = \delta(t - t')\delta^{(3)}(\mathbf{x} - \mathbf{x}') \quad (4.7)$$

Furthermore, the following decay chain can cause the fields in the strong  $\chi$  domain to decay into inflaton particles:

$$\chi \rightarrow yy\phi \quad (4.8)$$

During the period of inflation, this process allows for the establishment of a significant inflaton particle distribution, provided that the relation of the inflaton with the light degrees of freedom,  $y$ , in the thermal bath occurs rapidly enough. When observable CMB scales depart the horizon, the phase-space distribution  $n_*$  of the inflaton field determines the power spectrum [7, 13]:

$$\Delta_{\mathcal{R}}^2 = \left(\frac{H_*}{\dot{\phi}_*}\right)^2 \left(\frac{H_*}{2\pi}\right)^2 \left(1 + 2n_* + \frac{2\sqrt{3}\pi Q_*}{\sqrt{3 + 4\pi Q_*}} \frac{T_*}{H_*}\right) \quad (4.9)$$

Here, the symbol  $*$  denotes a quantity that is estimated at the time of the highest presently observable scales leaving the horizon. Additionally,  $n_* = n_{\text{BE}}(a_*H_*, T_*)$  represents the Bose-Einstein distribution for  $n_{\text{BE}}(k, T) = \frac{1}{e^{k/aT} - 1}$  at equilibrium. As  $n_*, Q_*, T_*$  approaches zero, the dimensionless power spectrum expression in cold inflation is regained. The power spectrum, for  $Q_* \ll 1$ , is given by:

$$\Delta_{\mathcal{R}}^2 \approx \left(\frac{H_*}{\dot{\phi}_*}\right)^2 \left(\frac{H_*}{2\pi}\right)^2 \left(1 + 2n_* + 2\pi Q_* \frac{T_*}{H_*}\right) \quad (4.10)$$

The term  $n_*$  precisely accounts for the impact of significant inflaton occupation numbers, while the dominant effect of fluctuation-dissipation dynamics is due to the term

$\left(1 + 2n_* + 2\pi Q_* \frac{T_*}{H_*}\right)$  that appeared in Eq. (4.10). The spectrum of primordial gravity waves remains unaffected by fluctuation-dissipation dynamics because of their low interaction with matter [5]. Therefore, the tensor spectrum maintains its form, as specified in Eq. (3.52). As a consequence, the value of  $r$  is decreasing which ultimately alters its connection to  $n_t = -2\epsilon_*$  from Eq. (3.53) as:

$$r \approx \frac{8|n_t|}{1 + 2n_* + 2Q_* T_*/H_*} \quad (4.11)$$

The investigation of dissipative effects during inflation demands a rigorous analysis of the scenario in which the generation of inflaton particles is not achieved rapidly enough. This scenario leads to a rapid redshift of any initial non-trivial occupation numbers by the inflationary expansion. The impact of  $n_* = 0$  can be neglected in our analysis even if the thermal bath of photons stays in equilibrium. The power spectrum  $\Delta_{\mathcal{R}}^2$ , for  $Q_* \ll 1$ , is described by the following expression [5]:

$$\Delta_{\mathcal{R}}^2 = \frac{V(\phi_*)}{24\pi\epsilon_*} \left(1 + \frac{2\pi Q_* T_*}{H_*}\right) \quad (4.12)$$

The scalar spectral index is obtained by using Eq. (4.12):

$$n_s \approx 1 + \frac{d \ln \Delta_{\mathcal{R}}^2}{d \ln k} \approx 1 - m_p^2 \frac{V_{,\phi}}{V} \frac{1}{\Delta_{\mathcal{R}}^2} \frac{d\Delta_{\mathcal{R}}^2}{d\phi} \approx 1 + 2\eta_* - 6\epsilon_* + \frac{2\kappa_*}{1 + \kappa_*} (7\epsilon_* - 4\eta_* + 5\sigma_*) \quad (4.13)$$

whereas  $\kappa_* = 2\pi Q_* \frac{T_*}{H}$  and tensor to scalar ratio would be given by:

$$r \approx \frac{16\epsilon_*}{1 + 2\pi Q_* \frac{T_*}{H_*}} \quad (4.14)$$

# Chapter 5

## The Principles of Hybrid Inflation

The universe's uniformity and isotropic behavior can be well explained by the inflation theory which demands a definite inflation model. Incorporating inflation with QFT helps to explain the precise aspects of the universe's post-inflation transition into the normal hot Big Bang era. This method also provides important new insights into the nature of temperature anisotropies in CMB radiation and small-density fluctuations that are the basis of the observable LSS in the cosmos. Note that the precise temperature anisotropy calculations might potentially distinguish between various particle physics models of inflation. The hybrid inflation model is considered among the most well-detailed cosmic inflationary models [4]. This model stands out due to its versatility in being consistently incorporated into different frameworks of high-energy physics such as SUSY, super-gravity, and GUT. It involves the coupling of one scalar field (inflaton) to another scalar field (the Higgs field).

This study aims to examine the chaotic potential, denoted as  $\lambda_p \phi^p$ , in the context of hybrid inflation. Specifically, tree-level predictions for different values of  $p$ , namely  $p = 1$  and  $2$ , are analyzed. These values correspond to well-motivated models of inflation [1]. It is notable that, generally, the inflaton can interact with both fermions and bosons. Previous studies [15] have examined how the inflaton's coupling to bosons affects the Higgs potential. However, the bosonic interaction leads to less favorable tree-level results [17]. In light of these developments, there is a compelling interest in investigating the prospects of  $A\phi^4 \ln(\phi)$  fermionic radiative corrections for  $A < 0$ .

The potential for tree-level hybrid inflation (TLHI) can be represented as a combination of the Higgs and the inflaton potential along with an interaction term  $g^2 \chi^2 \phi^2$  as:

$$V(\chi, \phi) = \kappa^2 \left( M^2 - \frac{\chi^2}{4} \right)^2 + \frac{g^2 \chi^2 \phi^2}{4} + \delta V(\phi) \quad (5.1)$$

where  $\kappa$  is a coupling constant,  $V(\chi)$  is the Higgs potential, and  $\delta V(\phi)$  is the inflaton potential. The inflaton potential is assumed to follow a chaotic polynomial-like form,

$\delta V(\phi) = \lambda_p \phi^p$  with  $p > 0$ . The interaction term ( $g^2 \chi^2 \phi^2$ ) in Eq. (5.1) serves the purpose of inducing an effective mass,

$$m_\chi^2 = -\kappa^2 M^2 + \frac{g^2 \phi^2}{2} = \frac{g^2}{2} (\phi^2 - \phi_c^2) \quad (5.2)$$

where  $\phi_c \equiv \sqrt{2\kappa}M/g$ . For the  $\chi$  field in the  $\chi = 0$  direction which represents a local minimum for  $\phi > \phi_c = \frac{\sqrt{2\kappa}M}{g}$  and is applicable for the inflation. Thus the effective single-field potential is provided by the following expression:

$$V(\phi) = (\kappa M^2)^2 + \delta V(\phi) = V_0 + \lambda_p \phi^p \quad (5.3)$$

where  $V_0 = \kappa^2 M^4$ . In this scenario, the chaotic potential plays a crucial role by providing the slope for the slowly rolling inflation within an otherwise flat valley. By establishing the appropriate initial conditions, one can ensure that inflation exclusively occurs within the  $\chi = 0$  valley until reaching  $\phi = \phi_c$ .

To delve into the predictions of the model, it's necessary to address the precise number of distinct factors. In addition to the  $\lambda_p$  factor associated with the potential in its chaotic form,  $\kappa$ ,  $M$ , and  $g$  are the primary potential factors in Eq. (5.1). One can reduce these factors to  $\phi_c$  and  $V_0$  in order to have an effective potential as given in Eq. (5.3). As the effective distinct factors, we use  $V_0$  and  $\kappa_c \equiv g^2/\kappa$  along with:

$$\phi_c = \sqrt{\frac{2V_0^{1/2}}{\kappa_c}} \quad (5.4)$$

This selection allows us to establish a straightforward correspondence with supersymmetric hybrid inflation, where  $\kappa_c = g = \kappa$ .

We now focus on the previously described model that has been radiatively adjusted. As stated earlier in this chapter, these corrections stem from potential interactions of the inflaton with different fields. Such interactions contribute to the restoration of the hot Big Bang phase beginning conditions during the reheating process. Fermionic and bosonic radiative corrections are the terms used to describe adjustments resulting from the inflaton's relations to fermions or bosons, respectively. We utilize the following simplified equation for the 1-loop Coleman-Weinberg potential in order to account for the effects of these modifications [9],

$$V_{1\text{-loop}} = A\phi^4 \ln\left(\frac{\phi}{\phi_c}\right) \quad (5.5)$$

where  $A < 0 (A > 0)$  illustrates the radiative corrections for fermionic (bosonic) systems. Although the chaotic inflation scenarios are characterized by quadratic and

quartic potentials, whereas fermionic radiative corrections are important too[16]. In general, fermionic radiative corrections tend to decrease both  $r$  and  $n_s$  in chaotic inflation scenarios. Consequently, we discuss the impact of fermionic radiative corrections on TL predictions in the next parts of the thesis and compare them with the most recent  $r$  and  $n_s$  constraints obtained from the Planck experiment.

The potential for radiatively corrected hybrid inflation at one-loop level (RCHI) can be expressed as [17],

$$V = V_0 + \lambda_p \phi^p - |A| \phi^4 \ln \left( \frac{\phi}{\phi_c} \right) \quad (5.6)$$

## 5.1 Quantitative Analysis

In this section, we did a comprehensive quantitative analysis of the hybrid model. The typical slow-roll parameters are used to derive estimations for the different inflationary factors.

$$\epsilon = \frac{1}{2(1+Q)} \left( \frac{m_P}{M} \right)^2 \left( \frac{V_{,\phi}}{V} \right)^2 \quad (5.7)$$

$$\eta = \frac{1}{2(1+Q)} \left( \frac{m_P}{M} \right)^2 \left( \frac{V_{,\phi\phi}}{V} \right) \quad (5.8)$$

$$\sigma^2 = \frac{1}{4(1+Q)^2} \left( \frac{m_P}{M} \right)^4 \left( \frac{V_{,\phi} V_{,\phi\phi\phi}}{V^2} \right) \quad (5.9)$$

Moreover, under the slow-roll approximation, the equations for  $n_s$  and  $r$  are expressed by Eq.(4.13) and (4.14). From the perspective of the  $\Lambda$ CDM model,  $n_s$  is reported as  $0.9665 \pm 0.0038$  [1]. One can find out the scalar power spectrum amplitude ( $A_s$ ) by using the following expression:

$$A_s = \frac{1}{24\pi^2 \epsilon(\phi_0)} \left( \frac{V(\phi_0)}{m_P^4} \right)$$

where  $k_0 = 0.05 \text{ Mpc}^{-1}$  is the pivot scale. A measurement provided by Planck [1], the amplitude is specified as  $A_s(k_0) = 2.137 \times 10^{-9}$  at the pivot scale ( $k_0$ ).

We take into account five separate important factors in our numerical evaluation:  $\kappa$ ,  $M$ ,  $\lambda$ ,  $\phi_0$ , and  $\phi_e$ . There are two primary limitations on these factors:

- The scalar power spectrum amplitude ( $A_s(k_0)$ ) is fixed i.e.  $2.137 \times 10^{-9}$ .
- The variable  $n_s$  with a constant value of 0.9665 [1].

When incorporating these constraints, we arrive at two distinct parameters, namely  $n_s$  and  $N$ , which can be manipulated independently. By fixing one of these parameters, we can systematically investigate the fluctuations in the other. In our analysis, we fixed  $N$  at 65. Since the relationship between  $n_s$  and  $r$  is crucial for testing inflationary models against observations, such as those from CMB radiation. The presence of the dissipation function and its effect on these plots suggests that these models include considerations of non-trivial dynamics during inflation, such as interactions between fields or with the thermal bath, which can alter the predictions of  $n_s$  and  $r$ .

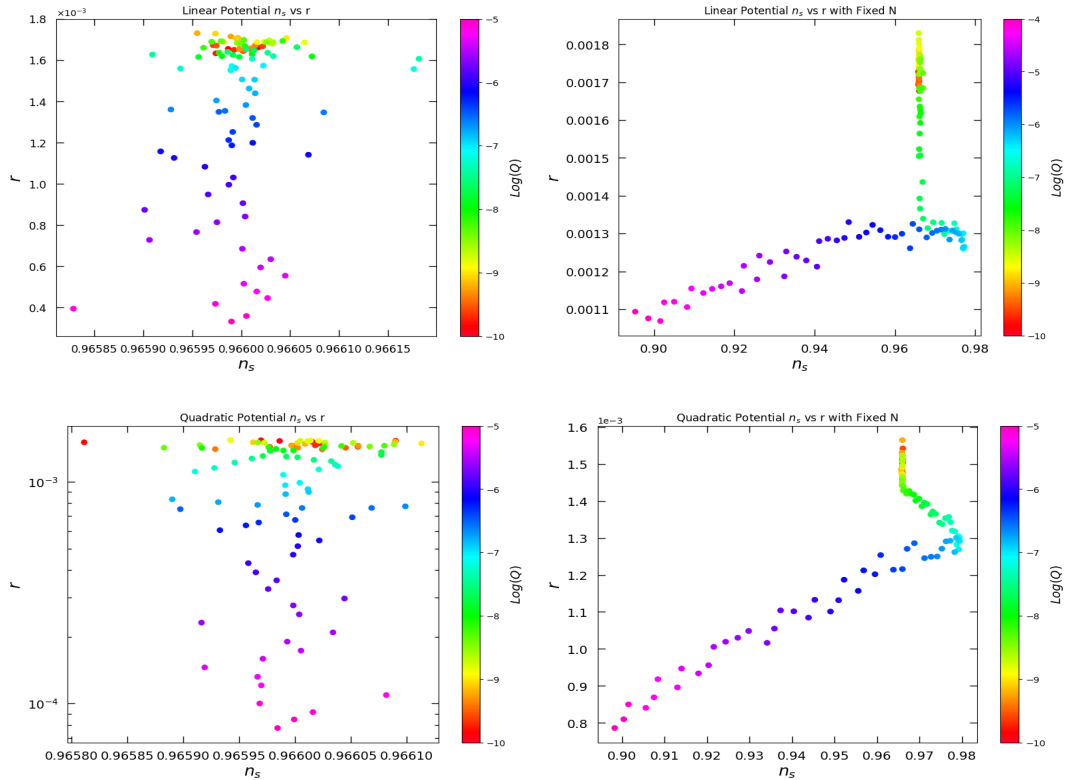


Figure 5.1:  $n_s$  vs  $r$  for linear and quadratic potential with color-coded  $\text{Log}(Q)$ . While in the two graphs,  $N$  is also taken as fixed i.e.  $N = 65$ .

We presented our numerical calculations in Figure 5.1, demonstrating the variations of parameters across the  $r - n_s$  plane. It depicts  $n_s - r$  plots, with the top two for linear and the bottom ones for quadratic potentials. The two left plots are with fixed  $n_s$  with one percent accuracy. The plots on the right number of e-folds  $N$  are fixed while  $n_s$  vary with  $Q$ . In the first and third graphs, for linear and quadratic potential respectively, the data points are scattered across a range of  $n_s$  and  $r$  values, with the color indicating the strength of the dissipation function. Most of the values of  $r$  lie within the range 0.0016–0.0018 for the value of  $n_s$  to be within the range 0.96595–0.96605. The spread

of the points suggests different outcomes for  $n_s$  and  $r$  based on the varying dissipation rates within the linear potential model of hybrid inflation. The second graph is more specific, showing  $n_s$  versus  $r$  for a fixed value of  $N$ . We observed that the value of  $r$  varies from 0.0013 – 0.0018 across a single value of  $n_s$  i.e. 0.9665 when the value of  $N$  is fixed at 65. This could mean that all these points correspond to models that predict the same amount of inflation but differ in other parameters.

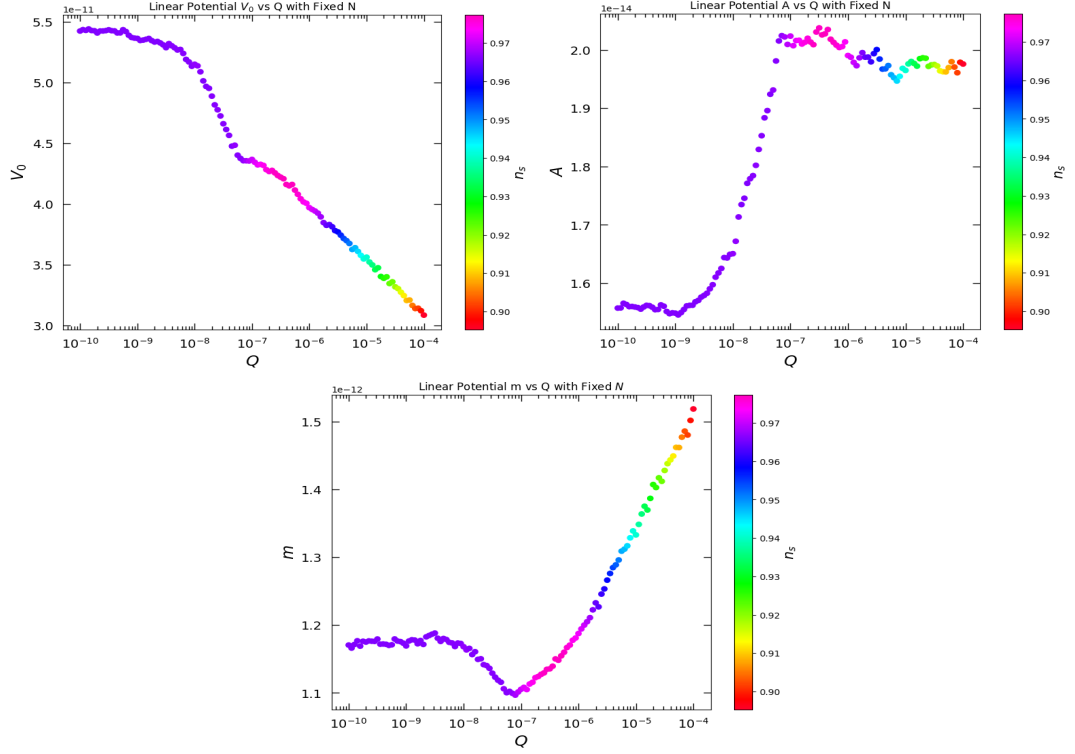


Figure 5.2:  $Q$  dependence on  $V_0$ ,  $A$ , and  $m$  with fixed  $N = 65$  and color-coded  $n_s$  ranging from 0.90 – 0.97 for linear potential.

Figure 5.2 illustrates the variation in dissipative ratio  $Q$  against effective potential  $V_0$ , radiative corrections  $A$ , and effective mass  $m$ , keeping  $N$  fixed at 65.

1.  **$V_0$  vs  $Q$  with Fixed  $N$  for linear potential:** Here, effective potential,  $V_0$ , is plotted against the dissipative ratio ( $Q$ ). The graph indicates a decrease in  $V_0$  with the value of  $Q$  varying from  $10^{-10}$  –  $10^{-4}$ , while  $n_s$  also vary across the spectrum from 0.90 to 0.97. This graph shows that the increase in the dissipative ratio causes a decrease in the effective potential which ultimately drives the inflation period towards the reheating.
2.  **$A$  vs  $Q$  with Fixed  $N$  for linear potential:** This graph shows the variation of  $A$  with the dissipative ratio ( $Q$ ). The value of the amplitude is initially constant

for  $Q = 10^{-10}$ . After this, the amplitude increases rapidly from  $1.6 \times 10^{-14}$  to  $2.0 \times 10^{-14}$  with  $Q$  merely changing from  $10^{-7}$  to  $10^{-8}$ . Afterward, the value of  $A$  fluctuates between  $1.9 \times 10^{-14}$  and  $2.0 \times 10^{-14}$  for  $Q$  going from  $10^{-4}$  to  $10^{-7}$ . The color gradient indicates the value of  $n_s$ , with  $A$  increasing with  $Q$  and  $n_s$  exhibiting a corresponding change.

3.  **$m$  vs  $Q$  with Fixed  $N$  for linear potential:** The graph plots the effective mass,  $m$ , of the inflaton, against  $Q$  ranging from  $10^{-10}$  to  $10^{-4}$ . Initially, the mass of inflation remains nearly  $1.2 \times 10^{-12}$  for  $Q$  varying from  $10^{-10}$  to  $10^{-7}$ . Afterward, it increases rapidly as we approach the end of inflation where  $Q = 10^{-4}$  follows a fluctuation at  $Q = 10^{-7}$ . The non-monotonic behavior of  $m$  as  $Q$  changes, alongside the variation in  $n_s$ , suggests a strong influence of the dissipation function on the inflationary dynamics.

The role of  $Q$  in hybrid inflation is critical. It adjusts how  $\phi$  interacts with other fields or the thermal bath, affecting inflation dynamics and the spectrum of primordial fluctuations. The results demonstrate the interplay between dissipation during inflation and observable cosmological parameters, providing testable predictions against CMB observations.

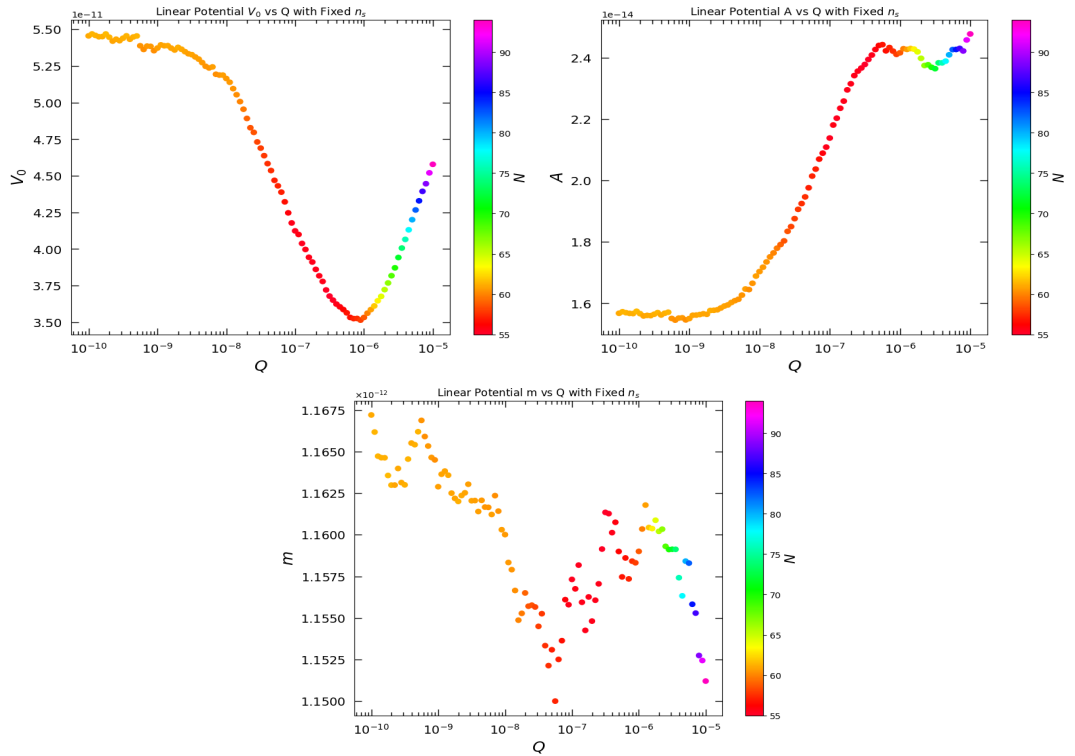


Figure 5.3:  $Q$  dependence on  $V_0$ ,  $A$ , and  $m$  with fixed  $n_s$  and color-coded  $N$  for linear potential.



Figure 5.3 illustrates the variation in dissipative ratio  $Q$  against effective potential  $V_0$ , radiative corrections  $A$ , and effective mass  $m$ , keeping  $n_s$  fixed.

1.  **$V_0$  vs  $Q$  with Fixed  $n_s$  for linear potential:** The plot displays  $V_0$  against  $Q$  at  $n_s = 0.9665$  for linear potential. With increasing  $Q$  from  $10^{-10}$  to  $10^{-6}$ , the value of  $V_0$  decreases to a minimum and then sharply increases. This shows the effective potential of the inflaton field as we approach the end of inflation. The color gradient suggests that this  $V_0$  minimum corresponds to a value of  $N$  from 55 – 60, the dissipation’s impact on inflationary dynamics is most significant at this range.
2.  **$A$  vs  $Q$  with Fixed  $n_s$  for linear potential:** This graph shows the variation of  $A$  with the change in the dissipative ratio  $Q$ . Initially  $A$  is constant with increasing  $Q$  from  $10^{-10}$  –  $10^{-8}$ , entering into a rapid increase with  $Q$  increasing up to  $10^{-6}$ . Afterward, the value of  $A$  is constant with slight fluctuations.
3.  **$m$  vs  $Q$  with Fixed  $n_s$  for linear potential:** Here  $m$  is plotted against  $Q$  for a fixed value of  $n_s$ . There is a non-linear relationship where  $m$  decreases with an increase in  $Q$  to a minimum value before rising again. The mass of the inflaton field fluctuates within a small range from 1.1500 to 1.1675 with an increase in the value of  $Q$  along with  $N$ . The color bar reveals that the minimum  $m$  corresponds to mid-range values of  $N$  i.e. from 60 to 75.

The graphs underscore the importance of  $Q$  in the dynamics of inflation, especially in scenarios where  $n_s$  is constant. They provide valuable insights into how dissipation affects the inflationary epoch’s duration and, consequently, the observable characteristics of the cosmic microwave background radiation.

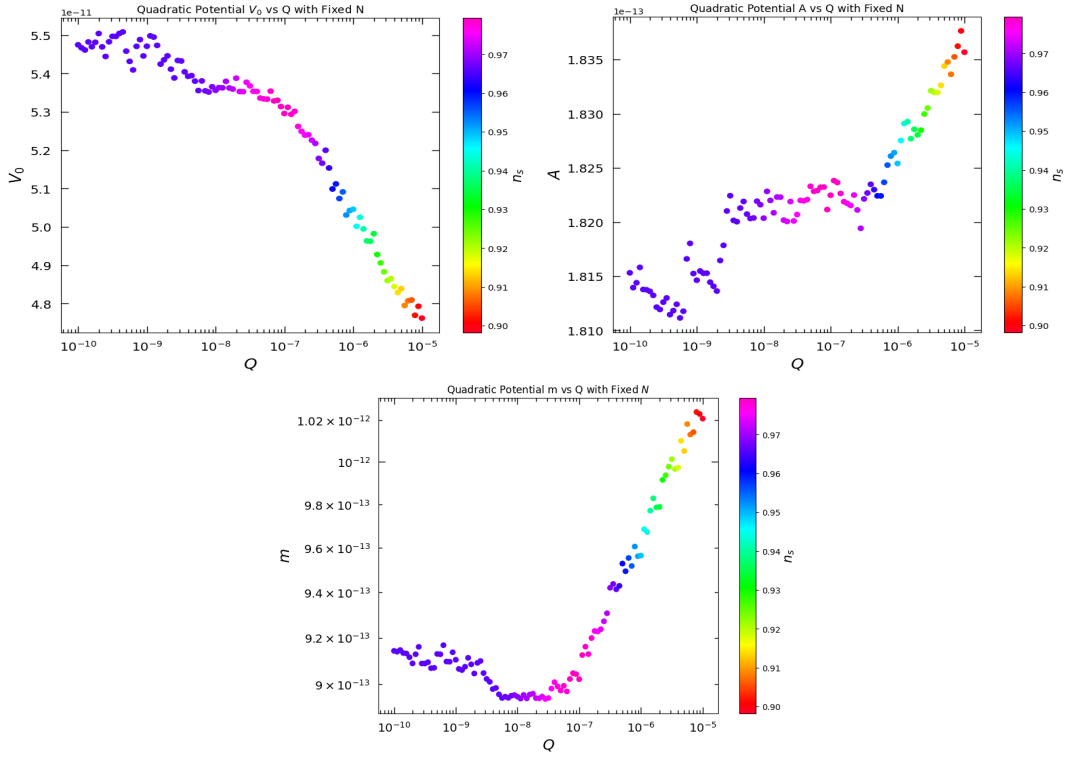


Figure 5.4:  $Q$  dependence on  $V_0$ ,  $A$ , and  $m$  with fixed  $N = 65$  and color-coded  $n_s$  ranging from 0.90 – 0.97 for quadratic potential.

Figure 5.4 illustrates the variation in dissipative ratio  $Q$  against effective potential  $V_0$ , radiative corrections  $A$ , and effective mass  $m$ , keeping  $N$  fixed at 65.

1.  **$V_0$  vs  $Q$  with Fixed  $N$  for quadratic potential:** The plot depicts  $V_0$  and how it varies with  $Q$  with  $N = 65$  for quadratic potential. The variation in the effective potential  $V_0$  is similar to the case of linear potential.  $V_0$  is initially constant and then decreases gradually with an increase in the value of  $Q$  as we approach the end of inflation.
2.  **$A$  vs  $Q$  with Fixed  $N$  for quadratic potential:** The graph displays  $A$  in relation to  $Q$  for quadratic potential. This graph also depicts different outcomes as of the linear potential. In case of quadratic potential, the value of  $A$  is increasing slowly rather than a rapid increase. It reaches the value of  $1.835 \times 10^{-13}$  as the universe approaches the end of inflation.
3.  **$m$  vs  $Q$  with Fixed  $N$  for quadratic potential:** This graph plots  $m$  against  $Q$  for quadratic potential. The value of  $m$  is less as compared to the value for linear potential but the trend in the variation of  $m$  against  $Q$  is the same as the

linear potential. Initially, its value is constant, and then at a certain range  $Q$ ,  $10^{-8}$  to  $10^{-7}$ , the inflaton mass (or a related parameter) reaches its minimum, constrained by a fixed  $N$ . Afterwards, it takes a sudden flight until the end of inflation approaches.

The trends in these graphs underscore the impact of dissipation mechanisms on the inflationary outcomes of a quadratic potential model. They demonstrate the influence of various dissipation strengths on the amplitude of primordial fluctuations, the inflaton's properties, and the initial potential energy, all within the framework of a fixed inflation duration. Understanding these relationships is vital for probing the physics of the early universe and comparing theoretical predictions with cosmic microwave background observations.

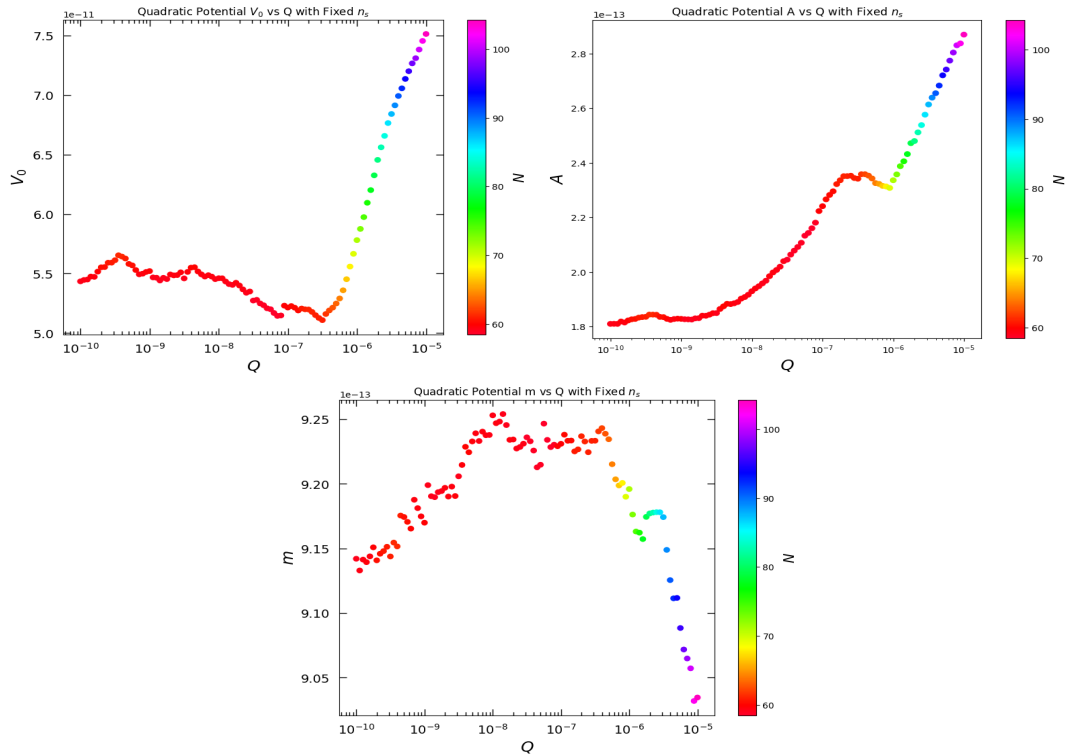


Figure 5.5:  $Q$  dependence on  $V_0$ ,  $A$ , and  $m$  with fixed  $n_s$  and color-coded  $N$  for quadratic potential.

Figure 5.5 illustrates the variation in dissipative ratio  $Q$  against effective potential  $V_0$ , radiative corrections  $A$ , and effective mass  $m$ , keeping  $n_s$  fixed.

1.  **$V_0$  vs  $Q$  with Fixed  $n_s$  for quadratic potential:** The graph of  $V_0$  against  $Q$  for quadratic potential. It shows a similar behavior as shown by the linear

potential. It demonstrates the value  $V_0$  fluctuates around  $5.5 \times 10^{-11}$  for a wide range of  $Q$ , from  $10^{-10}$  to  $10^{-6}$ . It then takes a rapid inclination in its value as it approaches the end of inflation. The color shifts demonstrate that these variations in  $V_0$  occur alongside alterations in  $N$  while maintaining  $n_s$  constant.

2.  **$A$  vs  $Q$  with Fixed  $n_s$  for quadratic potential:** This graph presents  $A$  against the dissipative ratio  $Q$  for quadratic potential. The value of  $A$  exhibits a sharp increase as  $Q$  grows from  $10^{-10}$  to  $10^{-6}$ , suggesting a potential regime shift in inflation. The color gradient indicates that this increase in  $A$  correlates with a rise in the value of  $N$ .
3.  **$m$  vs  $Q$  with Fixed  $n_s$  for quadratic potential:** The parameter  $m$ , representing the mass of the inflaton, shows a non-monotonic relationship with  $Q$ . As  $Q$  increases,  $m$  also increases, reaching a constant value before decreasing again, indicating complex behavior within the inflationary potential influenced by the dissipation rate. The color changes across the gradient suggest that these dynamics are associated with different durations of inflation.

These graphical representations elucidate the influence of dissipation, as quantified by  $Q$ , on crucial inflationary parameters in a quadratic potential scenario. Comprehending these interrelations is vital for the prediction of primordial fluctuation characteristics, which inform the LSS of the cosmos. To shed light on the mechanics of the early cosmos, these theoretical models are empirically verified against observational evidence, such as observations from the CMB.

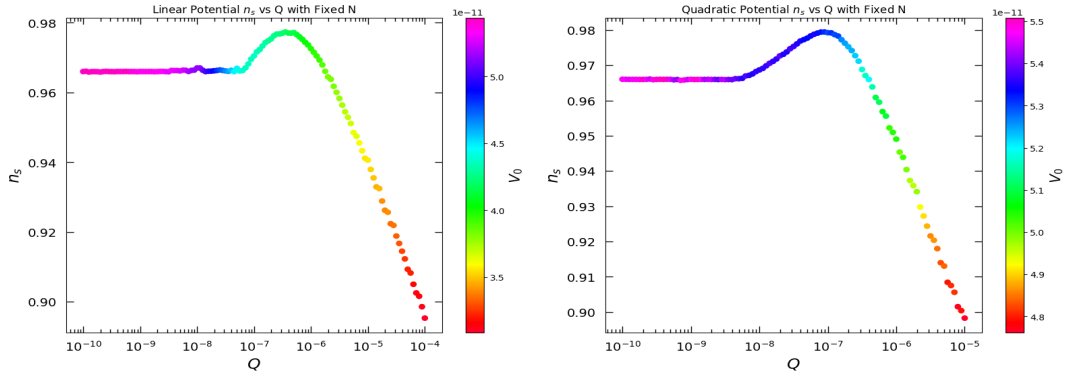


Figure 5.6:  $n_s$  vs  $Q$  for Linear and Quadratic potential with color-coded  $V_0$  and fixed  $N$ .

The graphs in Figure 5.6 depict  $n_s$  as a function of  $Q$  for two different inflationary potentials: linear and quadratic. The color bar represents the value of  $V_0$ , which could be the initial value of the inflationary potential or a scale associated with the potential.

1. **Linear Potential Graph  $n_s$  vs  $Q$  for fixed  $N$ :** The  $n_s$  value is fairly constant, 0.9665, over a range of  $Q$  values,  $10^{-10} - 10^{-7}$ , and then sharply decreases as  $Q$  increases. A decrease in  $V_0$  is observed with the decrease in  $n_s$  which indicates the universe to be approaching the radiation bath. For a linear potential in hybrid inflation,  $n_s$  is less sensitive to  $Q$  at lower values, indicating a threshold beyond which the potential's slope significantly affects the inflation dynamics.
2. **Quadratic Potential Graph  $n_s$  vs  $Q$  for fixed  $N$ :** This graph shows the same behavior as the linear potential graph. The  $n_s$  initially increases with  $Q$  and then decreases sharply. A similar decrease in  $V_0$  with the decrease in  $n_s$  is observed. The quadratic potential's curvature influences the inflationary dynamics, leading to a distinct relationship between  $n_s$  and  $Q$ .

In both cases, as  $Q$  increases,  $n_s$  decreases, reflecting the increased significance of quantum fluctuations or modifications to the inflation dynamics brought forth by the properties of the potential. The parameter  $Q$  might represent a ratio of field values, a coupling constant, or another characteristic of the inflationary model.

The variation of  $n_s$  with  $Q$  and  $V_0$  indicates that initial conditions and the potential significantly impact the predicted observational signatures of inflation. These predictions can be compared with observational data from the CMB to test the viability of different inflationary models.

# Chapter 6

## Conclusion

This dissertation has been dedicated to focusing primarily on warm inflation within the hybrid model formalism. The model investigated how dissipative and thermal factors impact the hybrid model of inflation's mechanics and empirical assumptions, which are influenced by radiative corrections. It is feasible to incorporate warm inflation into hybrid models, as the inflaton's interaction with the Higgs field affects the entire effective action controlling the inflaton field in addition to changing the effective potential. Consequently, the effective potential acquires a logarithmic gradient, coupled with the integration of a dissipation coefficient serving as a damping force in the motion equation for the inflaton. It leads to a decelerated progression of the inflaton field during the inflation, enabling a duration of 50 to 65 e-folds. Such a duration is compatible with a primordial spectrum that aligns with the findings from the Planck satellite at the Confidence Level of 95% [1]. We used fixed values of  $n_s$  and  $N$  that are given by the Planck Mission.

In the framework of the hybrid model, our primary focus was to examine the behavior of mass ( $m$ ), radiative corrections ( $A$ ), and effective potential ( $V_0$ ) for linear and quadratic cases that are directly coupled to the inflation field  $\phi$ . We demonstrated that incorporating these parameters significantly boosts the dissipation coefficient, particularly during the transition phase. Additionally, in our study, we distinctively accounted for dissipative effects for fixed  $n_s$  and  $N$ . In  $n_s - r$  plots,  $r$  is within the range of  $n_s$  which depicts the invariance of  $r$  w.r.t  $n_s$  for dissipative ratio ranging from  $10^{-6}$  to  $10^{-4}$  for linear and quadratic potential. For linear potential, the major contribution of  $V_0$ ,  $A$ , and  $m$  can be seen within the range of dissipative ratio ( $Q$ ) i.e.  $10^{-7} - 10^{-4}$  by fixing the value of  $n_s$  and  $N$  one by one. In the case of quadratic potential, the major contribution of these parameters can also be seen within the range of dissipative ratio ( $Q$ ) i.e.  $10^{-7} - 10^{-4}$  by fixing the value of  $n_s$  and  $N$  one by one.

Finally, the variation in the  $n_s$  w.r.t  $Q$  is observed with  $V_0$  also varying and fixed value of  $N$ . This is performed for both linear and quadratic potential. We can see that  $n_s$  is showing similar behavior for both types of potentials but at slightly different values

of  $V_0$ . The  $n_s$  value is the same for a range of the values of  $Q$  then it took a boost which ended soon and the value of  $n_s$  started decreasing gradually. This behavior of the spectral index is the same for linear and quadratic potentials.

# Appendix A

## Dynamics of the Warm Inflation

The dynamic behavior of the inflaton field, denoted by  $\phi(t)$ , in the context of standard supercooled inflation, is governed by a second-order differential equation:

$$\ddot{\phi}(t) + 3H\dot{\phi}(t) + V_{,\phi} = 0, \quad (\text{A.1})$$

The expression for  $H$ , which quantifies the expansion rate in the cosmos, is represented as:

$$H^2 = \frac{1}{3m_p^2} \left( \frac{\dot{\phi}^2}{2} + V(\phi) \right), \quad (\text{A.2})$$

assuming that the kinetic term  $\dot{\phi}^2/2$  is significantly lower than the potential term  $V(\phi)$ , i.e.,  $\dot{\phi}^2 \ll V(\phi)$ , the approximations  $3H^2m_p^2 \approx V(\phi)$  and  $\ddot{\phi}(t) \ll H\dot{\phi}(t)$  leads to a simplified equation of motion commonly referred to as the slow-roll approximation:

$$3H\dot{\phi} + V_{,\phi} = 0. \quad (\text{A.3})$$

The slow-roll parameter  $\epsilon$  is subsequently determined subject to the condition  $\dot{\phi}^2/2 < V(\phi)$  and using the approximations  $3H^2m_p^2 \approx V(\phi)$  and  $\ddot{\phi}(t) \ll H\dot{\phi}(t)$ , yielding:

$$\epsilon = \frac{m_p^2}{2(1+Q)} \left( \frac{V_{,\phi}}{V(\phi)} \right)^2 < 1. \quad (\text{A.4})$$

This formulation elucidates the conditions under which inflation occurs, emphasizing the dominance of the potential energy and the slow-roll behavior of the inflaton field. The parameter  $\eta$  is derived by differentiating the expression for  $\epsilon$ , which provides insight into the inflationary dynamics. The  $\eta$  parameter is expressed by:



$$\eta = \frac{m_p^2}{1+Q} \left( \frac{V_{,\phi\phi}}{V(\phi)} \right) < 1, \quad (\text{A.5})$$

In the realm of warm inflation, the typical equation of motion governing the behavior of the inflaton field is adjusted to include a dissipation coefficient, which functions as an additional frictional factor. This modification yields:

$$\ddot{\phi}(t) + (3H + \Gamma)\dot{\phi}(t) + V_{,\phi} = 0, \quad (\text{A.6})$$

The energy dissipated by the inflaton is transferred to another fluid component, with its evolution described by:

$$\dot{\rho} + 3H(\rho + p) = \Gamma(\dot{\phi}^2), \quad (\text{A.7})$$

This implies that energy is being transferred from the inflaton to this fluid component. If the dissipated inflaton energy quickly thermalizes into radiation, we denote  $\rho = \rho_R$  and  $p = p_R$ . The expression of  $\rho_R$  evolves according to:

$$\dot{\rho}_R + 4H\rho_R = \Gamma\dot{\phi}^2. \quad (\text{A.8})$$

In the slow-roll regime, the mathematical equations of motion for  $\rho_R$  and  $\phi$  are simplified by introducing the dissipative ratio  $Q = \Gamma/3H$ .

$$3H(1+Q)\dot{\phi} \approx -V_{,\phi}, \quad (\text{A.9})$$

$$4\rho_R \approx 3Q\dot{\phi}^2, \quad (\text{A.10})$$

These equations encapsulate the dynamics of the inflaton and radiation energy densities, incorporating dissipation and energy exchange in the context of warm inflation. In the context of warm inflation, the presence of the dissipative ratio  $Q$  leads to a modification of the slow-roll conditions, yielding:

$$\epsilon, |\eta| < (1+Q). \quad (\text{A.11})$$

This adaptation reflects the influence of dissipation on the inflationary dynamics. In the large field limit scenario, the low-momentum off-shell modes of mediator fields are the main source of the dissipation coefficient, as stated:

$$\Gamma = \frac{C_\phi T^3}{\phi^2}. \quad (\text{A.12})$$

From this,  $Q$  can be expressed as:

$$Q = \frac{C_\phi}{3} \left(\frac{T}{H}\right)^3 \left(\frac{H}{\phi}\right)^2. \quad (\text{A.13})$$

Utilizing the relation  $\rho_R = C_R T^4$ , where  $C_R = \frac{\pi^2 g_*}{30}$ , leads to the kinetic term of the inflaton:

$$\dot{\phi}^2 = 4C_R \left(\frac{T}{H}\right) H^4 \left(\frac{1}{C_\phi}\right) \left(\frac{\phi}{H}\right)^2. \quad (\text{A.14})$$

Upon integrating this aspect into the adjusted equation for the inflaton during the slow-roll phase, we obtain:

$$Q^{1/3}(1+Q)^2 = \frac{1}{(3H)^2} \left(\frac{C_\phi}{3}\right)^{1/3} \left(\frac{C_\phi}{4C_R}\right) \left(\frac{H}{\phi}\right)^{8/3} \frac{V'^2}{H^4}, \quad (\text{A.15})$$

which simplifies to:

$$Q^{1/3}(1+Q)^2 = 2\epsilon \left(\frac{C_\phi}{3}\right)^{1/3} \left(\frac{C_\phi}{4C_R}\right) \left(\frac{H}{\phi}\right)^{8/3} \left(\frac{m_p}{H}\right)^2. \quad (\text{A.16})$$

These equations illustrate the intricate relationship between the dissipative effects, characterized by  $Q$ , and the inflationary dynamics in the warm inflationary framework.

# Appendix B

## Equations of Motion for Warm Inflation

The initial expression describing the motion of  $\phi$  to the  $N_e$  is expressed as:

$$\frac{d}{dN_e} \left( \frac{\phi}{m_p} \right) = \frac{1}{H} \frac{d}{dt} \left( \frac{\phi}{m_p} \right). \quad (\text{B.1})$$

Utilizing the relationship  $\dot{\phi} = -\frac{V_{,\phi}}{3H(1+Q)}$ , the expression transforms into:

$$\frac{d}{dN_e} \left( \frac{\phi}{m_p} \right) = -\frac{\phi}{m_p} \frac{\sigma_\phi}{(1+Q)}, \quad (\text{B.2})$$

whereas the slow-roll parameter  $\sigma$  is introduced as:

$$\sigma = m_p^2 \frac{V_{,\phi}}{\phi V} \quad (\text{B.3})$$

The equation governing the evolution of the dissipative ratio, incorporating various derivatives, can be detailed as follows:

$$\frac{d}{dN_e} \epsilon = \frac{\epsilon}{1+Q} (4\epsilon - 2\eta), \quad (\text{B.4})$$

$$\frac{d}{dN_e} \left( \frac{m_p}{H} \right)^2 = \frac{2\epsilon}{1+Q} \left( \frac{m_p}{H} \right)^2, \quad (\text{B.5})$$

$$\frac{d}{dN_e} \left( \frac{H}{\phi} \right)^{\frac{8}{3}} = \left( \frac{8}{3}\sigma - \frac{8}{3}\epsilon \right) \frac{1}{1+Q} \left( \frac{H}{\phi} \right)^{\frac{8}{3}}. \quad (\text{B.6})$$

The differential of  $Q$  to the  $N_e$  is expressed as:

$$\frac{dQ}{dN_e} = \frac{Q}{1+7Q}(10\epsilon - 6\eta + 8\sigma). \quad (\text{B.7})$$

The Hubble parameter ( $H$ ) and temperature ( $T$ ) equation of motion, through the relationship, can be expressed as:

$$\left(\frac{T}{H}\right)^4 = \frac{3}{2C_R} \frac{Q}{(1+Q)^2} \epsilon \left(\frac{m_p}{H}\right)^2. \quad (\text{B.8})$$

Finally, the equation of motion for  $T/H$  to  $N_e$ , using the expressions for  $d(\phi/m_p)/dN_e$  and  $dQ/dN_e$ , is derived as:

$$\frac{d}{dN_e} \ln \left(\frac{T}{H}\right) = \frac{2}{1+7Q} \left( \frac{2+4Q}{1+Q} \epsilon - \eta + \frac{1-Q}{1+Q} \right). \quad (\text{B.9})$$

# References

- [1] P.A.R. Ade et al. “Planck 2018 results. X. Constraints on inflation.” In: (2018).
- [2] Mar Bastero-Gil and Arjun Berera. “Warm inflation dynamics in the low temperature regime.” In: *Phys.Rev.* D76 (2007), p. 043515.
- [3] Mar Bastero-Gil and Arjun Berera. “Warm inflation model building.” In: *Int.J.Mod.Phys.* A24 (2009), pp. 2207–2240.
- [4] Daniel Baumann. “TASI Lectures on Inflation.” In: (2009).
- [5] Micol Benetti and Rudnei O. Ramos. “Warm inflation dissipative effects: predictions and constraints from the Planck data”. In: *arXiv[1610.08758v1]*, (2016).
- [6] Arjun Berera and Li-Zhi Fang. “Thermally induced density perturbations in the inflation era.” In: *Phys.Rev.Lett.* 74 (1995), pp. 1912–1915.
- [7] Arjun Berera. “Thermal properties of an inflationary universe.” In: *Phys.Rev.* D54 (1996), pp. 2519–2534.
- [8] Arjun Berera. “Warm Inflation.” In: *Phys.Rev.Lett.* 75 (1995), pp. 3218–3221.
- [9] S. R. Coleman and E. J. Weinberg. “Radiative Corrections as the Origin of Spontaneous Symmetry Breaking,” in: *Phys. Rev. D* 7 (1973), p. 1888.
- [10] Scott Dodelson. “Modern Cosmology.” In: (2003).
- [11] Alan H. Guth. “The Inflationary Universe: A Possible Solution to the Horizon and Flatness Problems.” In: *Phys.Rev.* D23 (1981), pp. 347–356.
- [12] Andrew R. Liddle and D.H. Lyth. “Cosmological inflation and large scale structure.” In: (2000).
- [13] Andrei D. Linde. “A New Inflationary Universe Scenario: A Possible Solution of the Horizon, Flatness, Homogeneity, Isotropy and Primordial Monopole Problems.” In: *Phys.Lett.* B108 (1982), pp. 389–393.
- [14] H.P. de Oliveira and Rudnei O. Ramos. “Dynamical system analysis for inflation with dissipation.” In: *Phys.Rev.* D57 (1998), pp. 741–749.
- [15] M. U. Rehman and Q. Shafi. “Higgs Inflation, Quantum Smearing and the Tensor to Scalar Ratio,” in: *Phys. Rev. D* 81 (2010), p. 123525.

- [16] V. N. Senoguz and Q. Shafi. “Chaotic inflation, radiative corrections and precision cosmology,” in: *Phys. Lett. B* 668 (2008), p. 6.
- [17] Ommair Ishaque Waqas Ahmed and Mansoor Ur Rehman. “Quantum Smearing in Hybrid Inflation with Chaotic Potentials.” In: *arXiv:1501.00173v3* (2015).